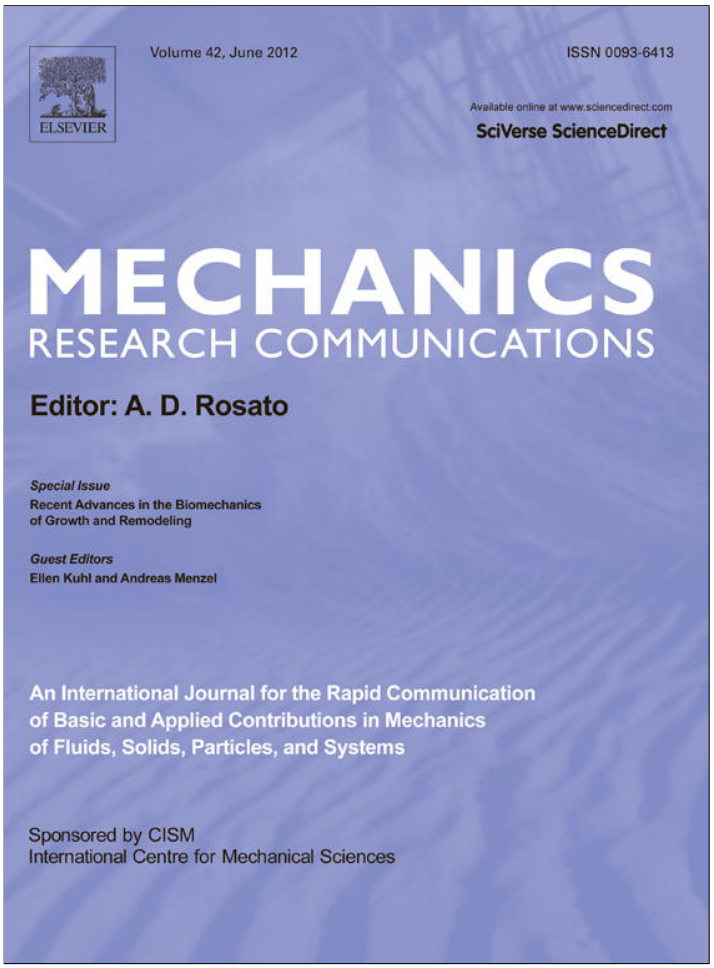

Mechanics Research Communications 42 (2012) 1–14

Contents lists available at SciVerse ScienceDirect

Mechanics Research Communications

journal homepage: www.elsevier.com/locate/mechrescom

Frontiers in growth and remodeling

Andreas Menzel[a,b], Ellen Kuhl[c,d,*]

[a] Institute of Mechanics, Department of Mechanical Engineering, TU Dortmund, Leonhard-Euler-Str. 5, D-44227 Dortmund, Germany
[b] Division of Solid Mechanics, Lund University, P.O. Box 118, SE-22100 Lund, Sweden
[c] Center of Mechanics, Department of Mechanical Engineering, ETH Zurich, Tannenstrasse 3, CH-8092 Zurich, Switzerland
[d] Departments of Mechanical Engineering, Bioengineering, and Cardiothoracic Surgery, Stanford University, 496 Lomita Mall, Stanford, CA 94305, USA

ARTICLE INFO

Article history:
Received 4 February 2012
Available online 3 March 2012

Keywords:
Living matter
Density growth
Volumetric growth
Area growth
Functional adaptation
Remodeling

ABSTRACT

Unlike common engineering materials, living matter can autonomously respond to environmental changes. Living structures can grow stronger, weaker, larger, or smaller within months, weeks, or days as a result of a continuous microstructural turnover and renewal. Hard tissues can adapt by increasing their density and grow strong. Soft tissues can adapt by increasing their volume and grow large. For more than three decades, the mechanics community has actively contributed to understand the phenomena of growth and remodeling from a mechanistic point of view. However, to date, there is no single, unified characterization of growth, which is equally accepted by all scientists in the field. Here we shed light on the continuum modeling of growth and remodeling of living matter, and give a comprehensive overview of historical developments and trends. We provide a state-of-the-art review of current research highlights, and discuss challenges and potential future directions. Using the example of volumetric growth, we illustrate how we can establish and utilize growth theories to characterize the functional adaptation of soft living matter. We anticipate this review to be the starting point for critical discussions and future research in growth and remodeling, with a potential impact on life science and medicine.

1. A brief history of growth and remodeling

In the century of quantitative biology, the mechanics community seems to keep ignoring the tremendous impact it could have on fusing live science and medicine by providing a unified, holistic, multiscale approach to characterize the fascinating features of living matter. On the small scale, biophysicists, who have long believed they could solve this challenging problem alone, are now coming to realize that their building block approach is inherently limited: nature is more than the sum of its parts. On the large scale, clinical researchers keep incrementally refining existing treatment strategies, with only few truly innovative advances. Their classical observational approach is undoubtably successful when comparing different treatment outcomes; yet, it fails to provide a mechanistic and predictive understanding of the underlying key phenomena. So what is the role that mechanics as a discipline could play in quantitative biology?

1.1. Where it all began: density growth of hard tissues

The fathers of modern biomechanics have impressively demonstrated that both biomechanics and mechanobiology play an important role when trying to understand biological form and function (Thompson, 1917; Wolff, 1870). On the one hand, biology can have a significant impact on mechanics: mechanical stiffness changes with biological microstructure. For almost half a century, we have known that these changes are not just linear, and that nature is more than the sum of its parts. Bone stiffness, for example, not only increases linearly with bone density, but exponentially, with exponents typically varying from two to three depending on the number and thickness of the individual trabaeculae (Carter and Hayes, 1977). These types of non-linearities are indeed very familiar to the mechanics community (Gibson and Ashby, 1997). We deal with geometric and constitutive non-linearities on a daily basis, and we know that superposition only holds in very few limited cases.

On the other hand, mechanics can have a tremendous impact on biology: biological microstructure changes with mechanical loading. Unlike engineering materials, living biological materials are not just constant throughout an individual's life time; they can adapt to environmental changes. Bone density, for example, changes in response to environmental forces, a phenomenon that has become known as the functional adaptation of bone (Cowin and Hegedus, 1977). For more than a century, researchers in different disciplines have been fascinated by this functional adaptation. Figs. 4 and 5

* Corresponding author at: Departments of Mechanical Engineering, Bioengineering, and Cardiothoracic Surgery, Stanford University, 496 Lomita Mall, Stanford, CA 94305, USA. Tel.: +1 6504500855.
E-mail address: ekuhl@stanford.edu (E. Kuhl).

0093-6413/$ – see front matter © 2012 Elsevier Ltd. All rights reserved.
doi:10.1016/j.mechrescom.2012.02.007

are only two out of many famous examples that illustrate how tissue microstructure is capable to align with the directions of maximum principal stress in the femur and in the tibia (Wolff, 1870). Non-constant densities are unconventional in classical mechanics, and we still struggle with characterizing them using our standard tools. Changes in mass, absolutely common in biology, require a characterization as a multi-phase material within the framework of mixture theories (Ateshian et al., 2012; Garikipati et al., 2004; Humphrey and Rajagopal, 2002) or as a single-phase material within the framework of open system thermodynamics (Epstein and Maugin, 2000; Kuhl and Steinmann, 2003a,b).

Hard tissues such as bone are admittedly a great model system to begin with, mainly for three reasons: first, since they do not undergo large deformations in vivo, a linear kinematics characterization is usually sufficiently accurate. Second, although they are multiphase materials consisting of solid and fluid constituents, for most technical applications, a single phase characterization in terms of the solid constituent alone represents their behavior sufficiently well (Kuhl et al., 2003). Third, since they are relatively easy to preserve, and their ex vivo response closely matches their in vivo behavior, they are relatively easy to test. This special issue provides a state-of-the-art overview on bone regeneration (Isaksson, 2012) and illustrates how we, as engineers, can adopt the design paradigms of nature when creating optimal, strong, and lightweight structures (Waffenschmidt and Menzel, 2012).

Overall, studying the functional adaptation of hard tissues has tremendously enhanced our understanding of bone density profiles in health and disease. We now know why astronauts lose bone in space (Kuhl and Steinmann, 2003c). We know why stiff implants used in hip replacement and repair induce a local loss of bone density through stress shielding (Ambrosi et al., 2011). We know why dental implants loosen over time in response to bone remodeling. We know that osteoporosis is associated with a local bone loss, which can be correlated to gait profiles (Pang et al., 2012). And we know why high-performance athletes in asymmetric sports, such as tennis players or baseball pitchers, have a significantly stronger dominant arm, in which they might develop chronic pain (Taylor et al., 2009).

1.2. Why it became complicated: volume growth of soft tissues

But why did we stop here? Translating what we know from hard tissues to soft is non-trivial for multiple reasons: First, soft tissues typically undergo large deformations and their accurate characterization requires a finite kinematic approach (Rodriguez et al., 1994). Second, their multi-phase character often plays a critical role, and their reduction to single-phase materials could sometimes be overly simplified (Mow et al., 1984). Third, they are difficult to preserve, and their ex vivo response might vary significantly from their in vivo behavior (Krishnamurthy et al., 2008). This difference might be attributed to residual stress (Alastrue et al., 2009a,b; Menzel, 2007; Taber and Humphrey, 2001) or to a pronounced active response (Famaey et al., in press; Itoh et al., 2009; Murtada et al., 2010).

Despite these challenges, a second generation of researchers in biomechanics has laid out a successful strategy how to characterize the living nature of soft biological tissues through iterative loops of establishing a theory, formulating testable hypotheses, designing experiments, probing the theory, calibrating the model parameters, and validating the model (Humphrey, 2002; Taber, 1995). Key to these developments was the re-interpretation of growth in terms of an incompatible configuration (Hsu, 1968; Skalak, 1981) and its mathematical characterization through the multiplicative decomposition of the deformation gradient into an elastic and a growth part (Goriely and BenAmar, 2007; Menzel, 2007; Rodriguez et al., 1994). This kinematic approach was soon recognized to enable the modeling of growth in various soft biological tissues (Garikipati, 2009; Lubarda, 2004). Fig. 6 illustrates one of the first attempts to utilize this concept and model isotropic volumetric growth of the arterial wall in response to balloon angioplasty and restenosis (Himpel et al., 2005; Kuhl et al., 2007). Within the past decade, several groups in mathematics and theoretical and applied mechanics have focused on formalizing the concept of volumetric growth, both within the frameworks of mixture theories (Ateshian et al., 2012; Garikipati et al., 2004) and open system thermodynamics (Chen and Hoger, 2000; Lubarda and Hoger, 2002; Menzel, 2005), and, only recently, within a combined framework of second order mass transport (Ciarletta et al., 2012). These attempts and recent trends are summarized in several illustrative overview articles (Ambrosi et al., 2011; Cowin, 2004; Verdier et al., 2009).

In addition to the mechanics community, the applied mathematics community has contributed tremendously to our understanding of growing soft biological tissues. Insightful theoretical contributions address the mathematical instabilities associated with growth (Ben Amar and Goriely, 2005), and the analytical solutions for growing plates (Dervaux et al., 2009), membranes (Goriely and Tabor, 2003; McMahon et al., 2010), and shells (Goriely and BenAmar, 2005). More applied contributions typically focus either on plant growth (Dumais et al., 2006; Vandiver and Goriely, 2009) or on clinically relevant growth (Ambrosi and Mollica, 2002). This special issue contains one application of the former class, growing pollen tube (Kroeger and Geitmann, 2012), and three of the latter class, growing tumors (Ambrosi et al., 2012), growing skin (Ciarletta and BenAmar, 2012), and growing cells in general (Ateshian et al., 2012).

Now that all these growth theories are more or less established, it is surprising that they attract so little attention. Why is it that the potential of growth theories is still underappreciated? Using growth theories to predict biological phenomena requires intense cross-talk between the different disciplines. We need to specify the individual growth laws for particular types of cells, plants, or tissues, isotropic, transversely isotropic, orthotropic, or generally anisotropic (Humphrey, 2001). We need to identify the driving forces for growth, stress, strain, or energy, and ideally tie them to the underlying mechanotransduction cascades that mediate the growth process (Jaalouk and Lammerding, 2009; Wong et al., 2011). And, most importantly, we need to identify relevant phenomena of growth in health and disease that warrant thorough investigation.

Typical health-relevant examples of volumetric growth are growing tumors (Ambrosi and Mollica, 2002; Ambrosi et al., 2010; Preziosi and Tosin, 2009) and growing mucous membranes (Li et al., 2011; Moulton and Goriely, 2011). Figs. 7 and 8 illustrates a health-relevant example of transversely isotropic growth characteristic for growing thin biological membranes such as skin (Buganza Tepole et al., 2011; Zöllner et al., in press). In contrast to tumor growth, here, growth is initiated on purpose to create extra tissue for defect correction in plastic and reconstructive surgery (Buganza Tepole et al., in press; Socci et al., 2007; Zöllner et al., 2012). This special issue also addresses another health-relevant example of biological growth in vision, with typical examples of glaucoma and myopia (Grytz et al., 2012).

The cardiovascular system undoubtably remains the prototype model system for soft tissue growth. Growth related phenomena in arteries have attracted both theoretical (Alford and Taber, 2008; Alford et al., 2008; Schmid et al., 2012) and computational (Alastrue et al., 2009a; Himpel et al., 2005) researchers equally, with characteristic problems as illustrated in Fig. 6. Two contributions of this special issue give insight into growing arterial tissue in general (Valentin and Holzapfel, 2012) and abdominal aortic aneurysms in particular (Zeinali-Davarani and Baek, 2012). A specific challenge is associated with the anisotropic nature of growth in cardiovascular tissue. Resent studies have characterized anisotropic growth

in response to myocardial infarction in vivo (Tsamis et al., 2012). Not only can the microstructural directions of anisotropy reorient themselves (Kuhl et al., 2005; Kuhl and Holzapfel, 2007; Menzel, 2005, 2007; Menzel and Waffenschmidt, 2009), as discussed in one contribution of this special issue (Pluijmert et al., 2012), but the tissue may also grow anisotropically in response to different loading scenarios (Göktepe et al., 2010a; Kerckhoffs et al., 2012). Cardiac muscle, for example, can grow isotropically (Kroon et al., 2009), undergo eccentric growth in response to volume overload (Göktepe et al., 2010b), or concentric growth in response to pressure overload (Rausch et al., 2011), as illustrated in Figs. 9 and 10. This special issue contains a collection of manuscripts related to the heart, to provide a state-of-the-art overview on cardiac growth in health and disease (Arts et al., 2012; Bellomo et al., 2012; Kerckhoffs et al., 2012; Klepach et al., 2012). Last, we discuss a possible reorientation of the underlying microstructure through the evolution of structural tensors (Himpel et al., 2008; Menzel, 2007) as illustrated in Fig. 11.

2. Kinematics of growth

Let us consider a body B embedded in the three-dimensional space. We distinguish between a chosen material or reference configuration $\mathcal{B}_0$ and the spatial or current configuration $\mathcal{B}_t$ of the body B. The spatial motion of referential position vectors of particles, $\boldsymbol{X} \in \mathcal{B}_0$, to their spatial position in $\mathcal{B}_t$ at time t is denoted by

$$\boldsymbol{x} = \boldsymbol{\varphi}(\boldsymbol{X}, t) \tag{1}$$

and is assumed to be sufficiently smooth; see Fig. 1 for a graphical illustration of the spatial motion problem. As this work proceeds, we will make use of the related gradient operations $\nabla_{\boldsymbol{X}}\{\circ\} = \mathrm{d}_{\boldsymbol{X}}\{\circ\}|_t$ and $\{\dot{\circ}\} = \mathrm{d}_t\{\circ\}|_{\boldsymbol{X}}$, with the latter referring to the material time derivative. When applying theses operations to Eq. (1), we obtain the well-established spatial motion deformation gradient and the spatial velocity,

$$\boldsymbol{F} = \nabla_{\boldsymbol{X}}\boldsymbol{\varphi} \quad \text{and} \quad \boldsymbol{v} = \dot{\boldsymbol{\varphi}}\,, \tag{2}$$

along with the spatial velocity gradient,

$$\boldsymbol{l} = \nabla_{\boldsymbol{x}}\boldsymbol{v} = \nabla_{\boldsymbol{X}}\boldsymbol{v}\cdot\boldsymbol{F}^{-1} = \dot{\boldsymbol{F}}\cdot\boldsymbol{F}^{-1}, \tag{3}$$

where $J = \det(\boldsymbol{F}) > 0$ so that $\boldsymbol{F}^{-1}$ exists. In complete analogy, we can consider the material motion problem

$$\boldsymbol{X} = \boldsymbol{\Phi}(\boldsymbol{x}, t) \tag{4}$$

and introduce the corresponding gradient operations $\nabla_{\boldsymbol{x}}\{\circ\} = \mathrm{d}_{\boldsymbol{x}}\{\circ\}|_t$ and $\{\mathring{\circ}\} = \mathrm{d}_t\{\circ\}|_{\boldsymbol{x}}$; see Fig. 1 for a graphical illustration of the kinematics of the material motion problem. When applying these operations to Eq. (4), we obtain the material motion deformation gradient and the material velocity,

$$\boldsymbol{f} = \nabla_{\boldsymbol{x}}\boldsymbol{\Phi} \quad \text{and} \quad \boldsymbol{V} = \mathring{\boldsymbol{\Phi}}\,, \tag{5}$$

along with the material velocity gradient,

$$\boldsymbol{L} = \nabla_{\boldsymbol{X}}\boldsymbol{V} = \nabla_{\boldsymbol{x}}\boldsymbol{V}\cdot\boldsymbol{f}^{-1} = \mathring{\boldsymbol{f}}\cdot\boldsymbol{f}^{-1} \tag{6}$$

where $j = \det(\boldsymbol{f}) > 0$ so that $\boldsymbol{f}^{-1}$ exists. Since $\boldsymbol{\Phi}$ is the inverse map of $\boldsymbol{\varphi}$, we can relate both formulations through $\boldsymbol{f} = \boldsymbol{F}^{-1}$ and $\boldsymbol{V} = -\boldsymbol{f}\cdot\boldsymbol{v}$.

2.1. Compatibility

We focus the subsequent brief discussion on compatibility-related properties of configurations. Here, we focus on the spatial motion problem, but identical relations hold for the material motion problem as $\boldsymbol{\Phi}(\boldsymbol{x}, t)$ is the inverse map of $\boldsymbol{\varphi}(\boldsymbol{X}, t)$. Since the deformation gradient represents the derivative of a vector potential, the related Piola identity is valid. In other words, the divergence of the cofactor of the deformation gradient vanishes identically,

$$\nabla_{\boldsymbol{X}}\cdot\mathrm{cof}(\boldsymbol{F}) = \boldsymbol{0}\,, \tag{7}$$

where $\mathrm{cof}(\boldsymbol{F}) = \mathrm{d}_{\boldsymbol{F}}J = J\ \boldsymbol{F}^{-\mathrm{t}}$ and $\nabla_{\boldsymbol{X}}\cdot\{\circ\}$ denotes the divergence operation. A general field representation of a second-order tensor includes further contributions in addition to the gradient form present in the definition of $\boldsymbol{F}$ in Eq. (2). To derive this general form, we consider the Helmholtz representation of a vector field,

$$\boldsymbol{h}(\boldsymbol{X}) = \nabla_{\boldsymbol{X}}a(\boldsymbol{X}) + \nabla^{\mathrm{t}}_{\boldsymbol{X}}\times\boldsymbol{b}(\boldsymbol{X}) + \boldsymbol{h}_c\,, \tag{8}$$

where $\nabla^{\mathrm{t}}_{\boldsymbol{X}}\times\{\circ\}$ denotes the curl operation and $\boldsymbol{h}_c$ is a constant vector (Dassiso and Lindel, 2001). A second-order tensor can be represented as $\boldsymbol{H}(\boldsymbol{X}) = \boldsymbol{h}_i(\boldsymbol{X})\otimes\boldsymbol{e}_i$, wherein $\boldsymbol{e}_i$ is a Cartesian base system, so that the application of Eq. (8) results in

$$\begin{aligned}\boldsymbol{H}(\boldsymbol{X}) &= \nabla_{\boldsymbol{X}}[a_i(\boldsymbol{X})\boldsymbol{e}_i] + \nabla^{\mathrm{t}}_{\boldsymbol{X}}\times[\boldsymbol{b}_i(\boldsymbol{X})\otimes\boldsymbol{e}_i] + \boldsymbol{H}_c\\ &= \nabla_{\boldsymbol{X}}\boldsymbol{a}(\boldsymbol{X}) + \nabla^{\mathrm{t}}_{\boldsymbol{X}}\times\boldsymbol{B}(\boldsymbol{X}) + \boldsymbol{H}_c\end{aligned} \tag{9}$$

with $\boldsymbol{H}_c = \text{const}$. When comparing the general field representation of a second-order tensor in Eq. (9) with the definition of $\boldsymbol{F}$ in Eq. (2), we conclude that the so-called incompatible part $\nabla^{\mathrm{t}}_{\boldsymbol{X}}\times\boldsymbol{B}$ is not activated and that, in consequence, Eq. (7) holds. We can further specify the vector field $\boldsymbol{a}(\boldsymbol{X})$ and the tensor field $\boldsymbol{B}(\boldsymbol{X})$ in Eq. (9) by means of the representations in Eqs. (8) and (9). This results in the representation

$$\boldsymbol{H}(\boldsymbol{X}) = \nabla^2_{\boldsymbol{X}\otimes\boldsymbol{X}}a(\boldsymbol{X}) + \nabla_{\boldsymbol{X}}[\nabla^{\mathrm{t}}_{\boldsymbol{X}}\times\boldsymbol{b}(\boldsymbol{X})] + \nabla^{\mathrm{t}}_{\boldsymbol{X}}\times[\nabla^{\mathrm{t}}_{\boldsymbol{X}}\times\boldsymbol{C}(\boldsymbol{X})] + \boldsymbol{H}_c \tag{10}$$

including the scalar, vector, and tensor potentials $a(\boldsymbol{X})$, $\boldsymbol{b}(\boldsymbol{X})$ and $\boldsymbol{C}(\boldsymbol{X})$. In order to make these potentials independent of each other, $\boldsymbol{b}(\boldsymbol{X})$ and $\boldsymbol{C}(\boldsymbol{X})$ must fulfill additional constraints. To give an example, when choosing the representation $\boldsymbol{C}(\boldsymbol{X}) = \boldsymbol{c}_i(\boldsymbol{X})\otimes\boldsymbol{e}_i$ the vector fields incorporated are constrained to be divergence-free, i.e., $\nabla_{\boldsymbol{X}}\cdot\boldsymbol{c}_i = \boldsymbol{0}$; for further background information and representations in view of related null Lagrangians (see Olver, 1993; Šilhavý, 1997). Applying the curl operation twice, such as $\nabla^{\mathrm{t}}_{\boldsymbol{X}}\times[\nabla^{\mathrm{t}}_{\boldsymbol{X}}\times\boldsymbol{C}(\boldsymbol{X})]$ in Eq. (10), is commonly denoted as the incompatibility operator frequently used in the context of continuum dislocation theories (Kröner, 1981; Lodge, 1974; Menzel and Steinmann, 2000).

2.2. Volume growth

The local evolution of material inhomogeneities, e.g., growth related to changes in volume and mechanical properties, can be interpreted as local material transformations or local deformation measures. Since the deformation gradient is a second-order tensor,

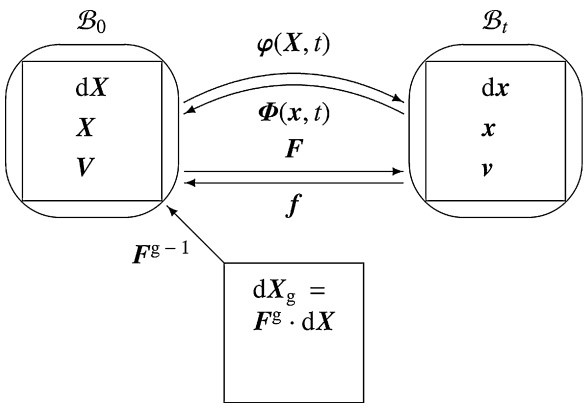

Fig. 1. Graphical illustration of the direct motion problem $\boldsymbol{\varphi}(\boldsymbol{X}, t)$ mapping referential particles $\boldsymbol{X}$ at time t onto their spatial position $\boldsymbol{x} = \boldsymbol{\varphi}(\boldsymbol{X}, t)$ and of the inverse motion problem $\boldsymbol{\Phi}(\boldsymbol{x}, t)$ mapping spatial particles $\boldsymbol{x}$ at time t onto their referential position $\boldsymbol{X} = \boldsymbol{\Phi}(\boldsymbol{x}, t)$. The local material transformation $\boldsymbol{F}^{g-1}$ maps infinitesimal line elements $\mathrm{d}\boldsymbol{X}_g$ at time t onto referential line elements $\mathrm{d}\boldsymbol{X} = \boldsymbol{F}^{g-1}\cdot\mathrm{d}\boldsymbol{X}$.

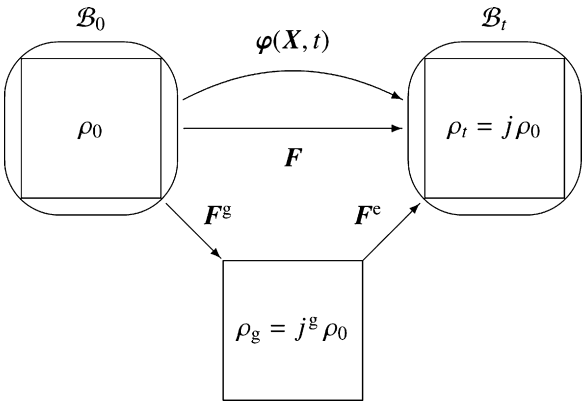

Fig. 2. Graphical illustration of the multiplicative decomposition of the deformation gradient $\boldsymbol{F} = \nabla_X \boldsymbol{\varphi} = \boldsymbol{F}^e \cdot \boldsymbol{F}^g$ into a reversible elastic part $\boldsymbol{F}^e$ and an irreversible growth part $\boldsymbol{F}^g$. The local mass density $\rho_t = j\rho_0$ and $\rho_g = j\rho_0$ are transformations of the referential density ρ_0 in terms of the Jacobians $j = \det(\boldsymbol{F}^{-1})$ and $j^g = \det(\boldsymbol{F}^{g-1})$.

we can replace $\boldsymbol{F}$ with $\boldsymbol{F} \cdot \boldsymbol{F}^{g-1}$, where $\boldsymbol{F}^g$ represents the local referential transformation; see Fig. 1. This modeling framework was first proposed in the context of general material inhomogeneities and finite elasto-plasticity (Lee, 1969; Noll, 1967) and, later on, applied in the context of growth (Rodriguez et al., 1994). The approach is commonly denoted as the multiplicative decomposition of the deformation gradient

$$\boldsymbol{F} = \boldsymbol{F}^e \cdot \boldsymbol{F}^g \tag{11}$$

into an energy-storing, reversible elastic part $\boldsymbol{F}^e$ and an irreversible growth part $\boldsymbol{F}^g$, with the related Jacobians

$$J^e = \det(\boldsymbol{F}^e) > 0 \quad \text{and} \quad J^g = \det(\boldsymbol{F}^g) > 0\,, \tag{12}$$

see Fig. 2. Unlike $\boldsymbol{F}$ in Eq. (2), neither $\boldsymbol{F}^e$ nor $\boldsymbol{F}^g$ can be derived from a vector field. Accordingly, unlike $\boldsymbol{F}$, neither $\boldsymbol{F}^e$ nor $\boldsymbol{F}^g$ do fulfill the Piola identity in Eq. (7). When applying the Helmholtz representation in Eq. (9) to $\boldsymbol{F}^e$ and $\boldsymbol{F}^g$, in general, the incompatible parts $\nabla^t_{\boldsymbol{X}} \times \boldsymbol{B}(\boldsymbol{X})$ do not vanish. In other words, $\boldsymbol{F}^e$ and $\boldsymbol{F}^g$ can not be defined as gradients of a vector potential. This implies that the interpretation of $\boldsymbol{F}^e$ and $\boldsymbol{F}^g$ as representing an additional global configuration is misleading. In view of the spatial motion problem, we can additively decompose the spatial velocity gradient

$$\boldsymbol{l} = \boldsymbol{l}^e + \boldsymbol{l}^g\,, \tag{13}$$

into an elastic and growth related part according to equation (11) with

$$\boldsymbol{l}^e = \dot{\boldsymbol{F}}^e \cdot \boldsymbol{F}^{e-1} \quad \text{and} \quad \boldsymbol{l}^g = \boldsymbol{F}^e \cdot \dot{\boldsymbol{F}}^g \cdot \boldsymbol{F}^{g-1} \cdot \boldsymbol{F}^{e-1}. \tag{14}$$

It proves convenient to also introduce their material counterparts $\boldsymbol{L}^e = \boldsymbol{F}^{e-1} \cdot \boldsymbol{l}^e \cdot \boldsymbol{F}^e$ and $\boldsymbol{L}^g = \boldsymbol{F}^{e-1} \cdot \boldsymbol{l}^g \cdot \boldsymbol{F}^e$ as

$$\boldsymbol{L}^e = \boldsymbol{F}^{e-1} \cdot \dot{\boldsymbol{F}}^e \quad \text{and} \quad \boldsymbol{L}^g = \dot{\boldsymbol{F}}^g \cdot \boldsymbol{F}^{g-1}, \tag{15}$$

where the growth velocity tensor $\boldsymbol{L}^g$ will play a key role in the formulation of constitutive equations in Section 4. We could also perform a similar transformation of $\boldsymbol{l}$ in terms of $\boldsymbol{F}$ instead of $\boldsymbol{F}^e$, but this would be less relevant in the sequel.

2.3. Surface growth

It is not always straightforward to distinguish between bulk and surface growth (Skalar et al., 1997). Let us consider a bar with equidistant markers and choose a cross-section Γ at one of its ends. Now, let the bar grow in longitudinal direction such that its end-to-end distance increases while its referential mass density and its cross-sectional area remain constant. If the distances between the markers remain constant and all markers move away from Γ, we classify the process as surface growth and conclude that the new material is supplied at the surface Γ. If the distances between the markers increase equally, we classify the process as bulk growth and conclude that the new material is supplied continuously within the bulk of the bar itself. Although the underlying mechanisms are fundamentally different, the final grown geometries could be entirely identical in both cases.

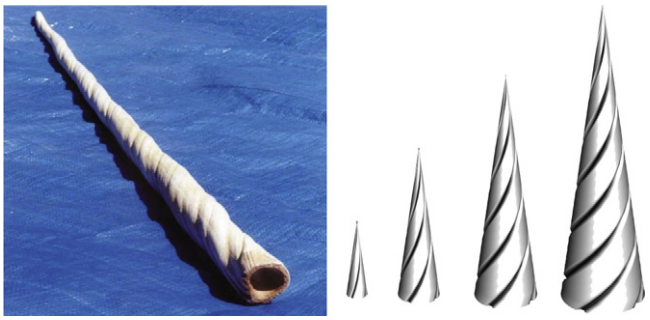

Fig. 3. Surface growth of a narwhal tusk with an upward pointing material velocity, $\boldsymbol{V} = \boldsymbol{V}^\Gamma + \boldsymbol{V}^g$, according to Eq. (16). Photograph of a narwhal tusk, left, demonstrates the characteristic helical growth pattern. Computational simulation of surface growth, right, with an outward pointing velocity $\boldsymbol{V}^\Gamma$ of the growth surface Γ, here characterized through the bottom ring, and a helically upward pointing velocity $\boldsymbol{V}^g$ of material grown at the surface Γ.

From a continuum mechanics point of view, Γ represents an internal surface with respect to which material moves in the case of surface growth. As such growth processes change the chosen reference configuration of the body, the velocities of material particles relative to the surface Γ can be best characterized in terms of the material motion problem (4). This motivates the additive decomposition of the material velocity $\boldsymbol{V}$ of a particle of the surface

$$\boldsymbol{V} = \boldsymbol{V}^\Gamma + \boldsymbol{V}^g \tag{16}$$

into the velocity $\boldsymbol{V}^\Gamma$ of the surface itself, and the velocity $\boldsymbol{V}^g$ of material grown at the surface Γ. Typical examples of surface growth include growing tusks, as shown in Fig. 3, horns, seashells, teeth (Skalar et al., 1997), and plant tips (Dumais et al., 2006; Kroeger et al., 2009) as discussed in Kroeger and Geitmann (2012) of this special issue.

Remark 1 *((Multiplicative decomposition)).* Kinematic approaches to finite inelasticity are frequently based on the multiplicative decomposition of the deformation gradient into an elastic and an inelastic part as suggested in Eq. (11). This approach was proposed in the context of finite crystal plasticity (Lee, 1969), where the multiplicative decomposition has a clear geometric interpretation and the so-called intermediate configuration is assumed to be stress-free. However, the decomposition (11) is not unique, since the rotational part can be chosen arbitrarily (Boyce et al., 1989; Naghdi, 1990). In view of finite growth, we apply the following polar decompositions

$$\boldsymbol{F}^e = \boldsymbol{v}^e \cdot \boldsymbol{R}^e \quad \text{and} \quad \boldsymbol{F}^g = \boldsymbol{R}^g \cdot \boldsymbol{U}^g$$

of the elastic part $\boldsymbol{F}^e$ into an elastic left stretch tensor $\boldsymbol{v}^e$ and an elastic rotation $\boldsymbol{R}^e$, and of the growth part $\boldsymbol{F}^g$ into a growth rotation $\boldsymbol{R}^g$ and a growth right stretch tensor $\boldsymbol{U}^g$. We can then combine the special orthogonal tensors $\boldsymbol{R}^e$ and $\boldsymbol{R}^g$ to a single rotation tensor $\boldsymbol{R}^{eg}$, such that

$$\boldsymbol{F} = \boldsymbol{F}^e \cdot \boldsymbol{F}^g = \boldsymbol{v}^e \cdot \boldsymbol{R}^e \cdot \boldsymbol{R}^g \cdot \boldsymbol{U}^g = \boldsymbol{v}^e \cdot \boldsymbol{R}^{eg} \cdot \boldsymbol{U}^g\,.$$

Based on the right polar decomposition of $\boldsymbol{F}^g$, the growth velocity tensor $\boldsymbol{L}^g$ takes the representation

$$\boldsymbol{L}^g = \boldsymbol{\Omega}^g + \boldsymbol{R}^g \cdot \dot{\boldsymbol{U}}^g \cdot \boldsymbol{U}^{g-1} \cdot \boldsymbol{R}^{gt}$$

with $\boldsymbol{\Omega}^{\mathrm{g}} = \dot{\boldsymbol{R}}^{\mathrm{g}} \cdot \boldsymbol{R}^{\mathrm{gt}} = -\boldsymbol{\Omega}^{\mathrm{gt}}$. If we restrict the growth tensor $\boldsymbol{F}^{\mathrm{g}}$ to be symmetric and a priori assume $\boldsymbol{F}^{\mathrm{g}} = \boldsymbol{U}^{\mathrm{g}}$, the spin $\boldsymbol{\Omega}^{\mathrm{g}}$ vanishes identically. If we additionally constrain the principal directions of $\boldsymbol{U}^{\mathrm{g}}$ to remain constant in time, e.g., referring to a prescribed orientation of the underlying microstructure, the growth velocity tensor $\boldsymbol{L}^{\mathrm{g}}$ turns out to be symmetric as well, i.e., $\boldsymbol{L}^{\mathrm{g}} = \boldsymbol{L}^{\mathrm{gt}}$.

3. Balance equations of growth

The balance equations of a growing body must account for possible changes in mass. This implies that the local referential mass density ρ_0 can change in response to a possible mass source R_0 and a possible mass flux $\boldsymbol{R}$. This implies that the balance equations of growing open systems may deviate from their standard representations for bodies with a constant mass. As this work proceeds, we briefly revisit some essential balance equations in the context of open system thermodynamics. Thereby, we restrict ourselves to the balance equations of the spatial motion problem for one single constituent, similar to Waffenschmidt and Menzel (2012) of this special issue, and neglect the additional interaction terms that would be present in general mixture theories. These are discussed in detail, e.g., in Ateshian et al. (2012) and Zeinali-Davarani and Baek (2012) of this special issue.

3.1. Balance of mass

The local form of the balance of mass for open systems balances the rate of change of the referential density $\dot{\rho}_0$ with a possible in- or outflux of matter $\boldsymbol{R}$ and a possible mass source R_0,

$$\dot{\rho}_0 = \nabla_{\boldsymbol{X}} \cdot \boldsymbol{R} + R_0 \,. \tag{17}$$

From a microscopic point of view, the mass flux can be associated with cell migration and the mass source can be related to cell proliferation, hyperplasia, hypertrophy, mitosis, necrosis, and apoptosis.

3.2. Balance of linear momentum

In the context of open system thermodynamics, we can distinguish between the volume- and mass-specific formats of all higher-order balance equation (Kuhl and Steinmann, 2003a). The volume specific form of the local spatial motion balance of linear momentum

$$\dot{\rho}_0 \boldsymbol{v} + \rho_0 \dot{\boldsymbol{v}} = \nabla_{\boldsymbol{X}} \cdot \boldsymbol{P} + \rho_0 \boldsymbol{b} \tag{18}$$

relates the rate of momentum $\dot{\rho}_0 \boldsymbol{v} + \rho_0 \dot{\boldsymbol{v}}$, the momentum flux $\boldsymbol{P}$, and the momentum source $\rho_0 \boldsymbol{b}$. Subtraction of the velocity-weighted version of Eq. (17) results in the reduced mass specific local formulation of the linear momentum balance,

$$\rho_0 \dot{\boldsymbol{v}} = \nabla_{\boldsymbol{X}} \cdot [\boldsymbol{P} - \boldsymbol{v} \otimes \boldsymbol{R}] + \rho_0 \boldsymbol{b} + R_0 \boldsymbol{v} + \dot{\boldsymbol{F}} \cdot \boldsymbol{R} \,, \tag{19}$$

which we will utilize in the sequel. By neglecting the mass flux, $\boldsymbol{R} = \boldsymbol{0}$, assuming a quasi-static setting, $\dot{\boldsymbol{v}} = \boldsymbol{0}$, and considering a separation of time scales as the speed of growth is significantly smaller than $\boldsymbol{v}$, such that $\boldsymbol{v} = \boldsymbol{0}$, we end up with the reduced representation

$$\boldsymbol{0} = \nabla_{\boldsymbol{X}} \cdot \boldsymbol{P} + \rho_0 \boldsymbol{b} \tag{20}$$

where $\boldsymbol{P}$ represents the standard Piola stresses.

3.3. Balance of entropy

To ensure that the overall dissipation remains non-negative, we discuss the local balance of entropy in form of the Clausius Duhem inequality. We assume that the temperature θ remains constant, which is a reasonable assumption for living biological tissues. The local form of the deformation-related part of the dissipation inequality for open systems reads

$$\rho_0 \mathcal{D} = \boldsymbol{P} : \dot{\boldsymbol{F}} - \rho_0 \dot{\psi} + \theta \; [\nabla_{\boldsymbol{X}} \cdot \boldsymbol{S} - S_0] \geq 0 \tag{21}$$

where $\psi_0 = \rho_0 \psi$ is the volume specific free energy density, and $\boldsymbol{S}$ and S_0 denote an extra external entropy flux and source to account for the living nature of biological systems (Kuhl and Steinmann, 2003a; Menzel, 2005).

Remark 2 *((Residual stresses)).* Biological tissues often possess so-called residual stresses, which we will denote as $\boldsymbol{P}^{\mathrm{res}}$. By following the outline and argumentation in (Holzapfel and Ogden, 2003, pp. 65–108), we make use of the relation

$$\nabla_{\boldsymbol{X}} \cdot [\boldsymbol{X} \otimes \boldsymbol{P}^{\mathrm{res}}] = \boldsymbol{X} \otimes [\nabla_{\boldsymbol{X}} \cdot \boldsymbol{P}^{\mathrm{res}}] + \nabla_{\boldsymbol{X}} \boldsymbol{X} \cdot \boldsymbol{P}^{\mathrm{rest}} \,. \tag{22}$$

Application of the divergence theorem to the integral form of Eq. (22) results in

$$\int_{\mathcal{B}_0} \boldsymbol{P}^{\mathrm{rest}} \; \mathrm{d}V = \int_{\partial \mathcal{B}_0} \boldsymbol{X} \otimes \boldsymbol{P}^{\mathrm{res}} \cdot \boldsymbol{N} \; \mathrm{d}A + \int_{\mathcal{B}_0} \boldsymbol{X} \otimes \nabla_{\boldsymbol{X}} \cdot \boldsymbol{P}^{\mathrm{res}} \; \mathrm{d}V \,, \tag{23}$$

with $\boldsymbol{N}$ denoting the outward referential unit vector. The residual stresses $\boldsymbol{P}^{\mathrm{res}}$ must fulfill the local form of the balance of linear momentum (20). By assuming the momentum source $\rho_0 \boldsymbol{b}$ to vanish, we conclude that the local equilibrium equation $\nabla_{\boldsymbol{X}} \cdot \boldsymbol{P}^{\mathrm{res}} = \boldsymbol{0}$ holds. Moreover, the surface integral in Eq. (23) must be identical to zero as external surface forces are excluded for the unloaded body considered. Accordingly, all integrals in (23) are zero and $\int_{\mathcal{B}_0} \boldsymbol{P}^{\mathrm{res}} \; \mathrm{d}V = \boldsymbol{0}$ implies either that $\boldsymbol{P}^{\mathrm{res}} = \boldsymbol{0}$ or that $\boldsymbol{P}^{\mathrm{res}}$ is distributed inhomogeneously within $\mathcal{B}_0$. Note that the growth related part $\boldsymbol{F}^{\mathrm{g}}$ allows to conveniently include residual stresses at vanishing local strains, i.e., $\boldsymbol{F} = \boldsymbol{I}$; see Section 4.3 below. For further background information on the incorporation of residual stresses as additional arguments in the constitutive equations, we refer the reader to Hoger (1996) and references cited therein. Typical experiments to demonstrate residual stresses in growing tissue are the classical opening angle experiment, e.g., in arteries (Famaey et al., in press), and peeling of living bilayers, which grow at different rates, e.g., in rhubarb (Vandiver and Goriely, 2009).

4. Constitutive equations of growth

To close the systems of equations, we must introduce constitutive relations for the source terms R_0, S_0, $\boldsymbol{b}$ as well as for the flux terms $\boldsymbol{R}$, $\boldsymbol{S}$, $\boldsymbol{P}$, and, if present, for the evolution of internal variables. Here, we will neither provide a specific representation for $\boldsymbol{b}$, such as volume forces resulting from gravity, nor for the external entropy flux $\boldsymbol{S}$ and entropy source S_0, which we simply assume to take values such that inequality (21) is satisfied. In order to evaluate the dissipation inequality (21), we first specify the free energy

$$\psi(\boldsymbol{F}, \boldsymbol{F}^{\mathrm{g}}, \boldsymbol{A}^P, \rho_0, \theta) = \widetilde{\psi}(\boldsymbol{F}^{\mathrm{e}}, \boldsymbol{A}^P, \rho_0, \theta) \,, \tag{24}$$

where we have admitted the explicit dependency on $\boldsymbol{X}$ to simplify the notation. The additional variable $\boldsymbol{A}^P$ constitutes a so-called structural tensor to account for a possible anisotropic elastic behavior. A typical assumption for this tensor is a symmetric rank one form, $\boldsymbol{A}^P = \boldsymbol{a}^P \otimes \boldsymbol{a}^P$, where the vector $\boldsymbol{a}^P$ characterizes a specific direction of anisotropy. Here, we focus on only one structural tensor and refer to Menzel (2007) for a growth model including anisotropic elasticity with multiple structural tensors. Using Eqs. (17) and (24), and assuming $\dot{\theta} = 0$, we can re-write the dissipation inequality in the following form.

$$\rho_0 \mathcal{D} = \left[\boldsymbol{P} - \rho_0 \frac{\partial \psi}{\partial \boldsymbol{F}} \right] : \dot{\boldsymbol{F}} - \rho_0 \frac{\partial \psi}{\partial \boldsymbol{F}^{\mathrm{g}}} : \dot{\boldsymbol{F}}^{\mathrm{g}} - \rho_0 \frac{\partial \psi}{\partial \boldsymbol{A}^P} : \dot{\boldsymbol{A}}^P - \rho_0 \frac{\partial \psi}{\partial \rho_0} [\nabla_{\boldsymbol{X}} \cdot \boldsymbol{R} + R_0] + \theta [\nabla_{\boldsymbol{X}} \cdot \boldsymbol{S} - S_0] \geq 0. \tag{25}$$

In the following subsections, we will use this dissipation inequality to specify functional dependencies of the mass source, the mass flux, the momentum flux, and the evolution of growth.

4.1. Mass source

In general, the mass source R_0 is a scalar-valued tensor function of the state variables, their material time derivatives, and additional arguments to be specified. When neglecting the introduction of additional arguments, such as additional structural tensors, rates, and gradients of the state variables, the mass source function may take the following representation

$$R_0(\boldsymbol{F}, \boldsymbol{F}^{\mathrm{g}}, \boldsymbol{A}^P, \rho_0, \theta). \tag{26}$$

4.2. Mass flux

In analogy to the mass source, the mass flux $\boldsymbol{R}$ is a vector-valued tensor function of the state variables, their rates, their gradients, and additional arguments to be specified. We assume $\boldsymbol{R}$ to be independent of the rates of the state variables, but formally introduce another tensorial variable $\boldsymbol{A}^R$ and include only one additional gradient contribution, namely the gradient of the referential mass density. As a result, the mass flux function may take the following representation

$$\boldsymbol{R}(\boldsymbol{F}, \boldsymbol{F}^{\mathrm{g}}, \boldsymbol{A}^P, \boldsymbol{A}^R, \rho_0, \nabla_{\boldsymbol{X}} \rho_0, \theta). \tag{27}$$

4.3. Momentum flux

To introduce the momentum flux in a thermodynamically motivated way, we explore the first term of the dissipation inequality (25). We adopt a hyperelastic format to define the momentum flux, and introduce the Piola stress $\boldsymbol{P}$ as energetically conjugate to the rate of the deformation gradient $\dot{\boldsymbol{F}}$, i.e.,

$$\boldsymbol{P} = \rho_0 \frac{\partial \psi}{\partial \boldsymbol{F}} = \boldsymbol{P}^{\mathrm{e}} \cdot \boldsymbol{F}^{\mathrm{g-t}} \quad \text{with} \quad \boldsymbol{P}^{\mathrm{e}} = \rho_0 \frac{\partial \widetilde{\psi}}{\partial \boldsymbol{F}^{\mathrm{e}}}. \tag{28}$$

This implies that the first term of the dissipation inequality (25) vanishes identically for all $\dot{\boldsymbol{F}}$.

4.4. Evolution of growth

To characterize the evolution of growth, we explore the second term of the dissipation inequality (25). In analogy to considerations common in finite strain plasticity,

$$\begin{aligned} -\rho_0 \frac{\partial \psi}{\partial \boldsymbol{F}^{\mathrm{g}}} : \dot{\boldsymbol{F}}^{\mathrm{g}} &= -\left[\rho_0 \frac{\partial \psi}{\partial \boldsymbol{F}^{\mathrm{g}}} \cdot \boldsymbol{F}^{\mathrm{gt}} \right] : \left[\dot{\boldsymbol{F}}^{\mathrm{g}} \cdot \boldsymbol{F}^{\mathrm{g-1}} \right] \\ &= -\left[\boldsymbol{P}^{\mathrm{e}} : \frac{\partial \boldsymbol{F}^{\mathrm{e}}}{\partial \boldsymbol{F}^{\mathrm{g}}} \cdot \boldsymbol{F}^{\mathrm{gt}} \right] : \boldsymbol{L}^{\mathrm{g}} \\ &= \left[\boldsymbol{F}^{\mathrm{et}} \cdot \boldsymbol{P}^{\mathrm{e}} \right] : \boldsymbol{L}^{\mathrm{g}} = \boldsymbol{M}^{\mathrm{e}} : \boldsymbol{L}^{\mathrm{g}}, \end{aligned} \tag{29}$$

We introduce the Mandel stresses $\boldsymbol{M}^{\mathrm{e}} = \boldsymbol{F}^{\mathrm{et}} \cdot \boldsymbol{P}^{\mathrm{e}}$ as thermodynamically conjugate to the growth velocity tensor $\boldsymbol{L}^{\mathrm{g}}$. These thermodynamic considerations motivate to introduce the evolution of the growth tensor $\dot{\boldsymbol{F}}^{\mathrm{g}}$ in form of $\boldsymbol{L}^{\mathrm{g}}$ to be a function of the Mandel stresses $\boldsymbol{M}^{\mathrm{e}}$ and additional variables such as a structural-tensor-type quantity $\boldsymbol{A}^{\mathrm{g}}$, i.e.,

$$\boldsymbol{L}^{\mathrm{g}}(\boldsymbol{M}^{\mathrm{e}}, \boldsymbol{A}^{\mathrm{g}}, \rho_0, \theta). \tag{30}$$

Since $\boldsymbol{L}^{\mathrm{g}}$ is assumed to depend on $\boldsymbol{M}^{\mathrm{e}}$, the particular type of evolution Eq. (30) is, by analogy, similar to models in finite plasticity, here denoted as stress-driven growth. Alternatively, we could consider an ad hoc introduction of $\boldsymbol{L}^{\mathrm{g}}$, i.e., not motivated by direct thermodynamical considerations, for example in a strain-driven format,

$$\boldsymbol{L}^{\mathrm{g}}(\boldsymbol{F}, \boldsymbol{F}^{\mathrm{g}}, \boldsymbol{A}^{\mathrm{g}}, \rho_0, \theta). \tag{31}$$

4.5. Evolution of structural tensor

In analogy to the evolution of $\boldsymbol{F}^{\mathrm{g}}$, the evolution of the structural tensor $\boldsymbol{A}^P$ can be introduced in a stress-driven form,

$$\dot{\boldsymbol{A}}^P(-\rho_0 \, \partial_{\boldsymbol{A}^P} \psi, \boldsymbol{A}^P, \rho_0, \theta) \tag{32}$$

where $-\rho_0 \, \partial_{\boldsymbol{A}^P} \psi$ takes the interpretation as stress-type tensor conjugate to $\boldsymbol{A}^P$, or in a strain-driven form,

$$\dot{\boldsymbol{A}}^P(\boldsymbol{F}, \boldsymbol{F}^{\mathrm{g}}, \boldsymbol{A}^P, \rho_0, \theta). \tag{33}$$

Alternatively, since $\boldsymbol{A}^P = \boldsymbol{a}^P \otimes \boldsymbol{a}^P$, we could introduce evolution equations for the microstructural vector $\dot{\boldsymbol{a}}^P$ itself, instead of its structural tensor $\dot{\boldsymbol{A}}^P$. This would then allow us to separately address the evolution of its length $||\boldsymbol{a}^P||$ and the evolution of its orientation of $\boldsymbol{a}^P$. In particular, when tying these evolution equations to observable variables, evolution equations for the microstructural vector $\dot{\boldsymbol{a}}^P$ might be more illustrative. The tensor functions in Eqs. (32) and (33) are assumed not to include further structural tensors such as $\boldsymbol{A}^R$ and $\boldsymbol{A}^{\mathrm{g}}$ which, in general, could also be included. Moreover, $\boldsymbol{A}^R$ and $\boldsymbol{A}^{\mathrm{g}}$ may also evolve with time, and follow evolution equations of similar forms as introduced in (32) and (33). Evolving structural tensors are typically used to characterize remodeling effects when the living structure undergoes changes is anisotropic material properties such as microstructural reorientations, see Himpel et al. (2008), Kuhl et al. (2005), Menzel (2007), or Pluijmert et al. (2012) of this special issue.

Remark 3 *((Thermodynamically conjugate pairs))*. Using the dissipation inequality (25), we have identified the Piola stress $\boldsymbol{P}$ and the rate of the deformation gradient $\dot{\boldsymbol{F}}$ as thermodynamically conjugate pairs in Section 4.3. In addition, we have identified the elastic Mandel stress $\boldsymbol{M}^{\mathrm{e}}$ and the growth velocity tensor $\boldsymbol{L}^{\mathrm{g}}$ as thermodynamically conjugate pairs in Section 4.4. Alternatively, we could have introduced the growth part of the Piola stress, $\boldsymbol{P}^{\mathrm{g}} = -\rho_0 \partial \psi / \partial \boldsymbol{F}^{\mathrm{g}}$, and the rate of the growth tensor $\dot{\boldsymbol{F}}^{\mathrm{g}}$ as conjugate pairs. In analogy to Eq. (30), this format would then motivate the introduction of the following evolution of growth,

$$\dot{\boldsymbol{F}}^{\mathrm{g}}(\boldsymbol{P}^{\mathrm{g}}, \boldsymbol{A}^{\mathrm{g}}, \rho_0, \theta),$$

as a function of the growth related Piola-type stresses, $\boldsymbol{P}^{\mathrm{g}}$, and all other variables, i.e., $\boldsymbol{A}^{\mathrm{g}}$, ρ_0, and θ.

5. Examples

In the previous section, we have introduced generalized functional forms of the constitutive equations, which characterize growth. Now, we will specify and discuss some particular examples. As such, this section is by far not intended to be complete; it is rather meant to provide guidelines and common practise when modeling particular types of growth. For simplicity, we restrict ourselves to transversely isotropic materials with one pronounced structural direction $\boldsymbol{a}$, such that the structural tensors of the baseline elastic

response $\boldsymbol{A}^P$, of the density distribution $\boldsymbol{A}^R$, and of volume growth $\boldsymbol{A}^g$ coincide.

$$\boldsymbol{A}^P \equiv \boldsymbol{A}^R \equiv \boldsymbol{A}^g \doteq \boldsymbol{A} \doteq \boldsymbol{a} \otimes \boldsymbol{a} \,. \tag{34}$$

Here, we will neither focus on the introduction of several or higher-order structural tensors, nor on the introduction of dispersion parameters or so-called orientation distribution functions; for further background information see Menzel (2007), Menzel et al. (2008), Menzel and Waffenschmidt (2009) and Harrysson et al. (2010) and references cited therein.

5.1. Mass source

The mass source R_0 in Eq. (26) may take different specific forms. One possibility is to make use of the transformation of the local mass densities in terms of the determinants of individual contributions of the deformation gradient. For the special case that the mass density remains constant upon growth, $\rho^g = \text{const}$, we can express the referential mass density ρ_0 as a function of the growth tensor $\boldsymbol{F}^g$. This implies that

$$\rho_0 = J^g \, \rho^g \quad \text{and} \quad \rho^g = j^g \, \rho_0 \,, \tag{35}$$

where ρ^g is the mass density related to the local transformation $\boldsymbol{F}^g$, $J^g = \det(\boldsymbol{F}^g)$, and $j^g = 1/J^g$, see Fig. 2. Recall that $J^g > 1$ implies a growth-related volume increase and $j^g > 1$ implies a volume reduction, i.e., positive and negative growth. Assuming a constant transformed mass density, $\rho^g = \text{const}$, and thus

$$\dot{\rho}^g = \dot{j}^g \, \rho_0 + j^g \, \dot{\rho}_0 = 0 \tag{36}$$

we can extract the following evolution equation for the referential mass density ρ_0,

$$\begin{aligned} \dot{\rho}_0 &= -\rho_0 \;\; J^g \dot{j}^g = -\rho_0 \;\; J^g \frac{\partial j^g}{\partial \boldsymbol{F}^{g-1}} : \dot{\boldsymbol{F}}^{g-1} \\ &= -\rho_0 \;\; \boldsymbol{F}^{gt} : \dot{\boldsymbol{F}}^{g-1} = \rho_0 \;\; \text{tr}(\boldsymbol{L}^g) \end{aligned} \tag{37}$$

with $\dot{\boldsymbol{F}}^g \cdot \boldsymbol{F}^{g-1} = -\boldsymbol{F}^g \cdot \dot{\boldsymbol{F}}^{g-1}$ and the trace operation $\text{tr}\{\circ\} = \{\circ\} : \boldsymbol{I}$ where $\boldsymbol{I}$ denotes the second-order identity tensor. For most biological tissues, it is a reasonable assumption that the mass flux $\boldsymbol{R}$ is constant in space, i.e., $\nabla_X \cdot \boldsymbol{R} = 0$. In this special case, Eq. (17) implies that the rate of the referential mass density $\dot{\rho}_0$ is identical to the mass source R_0, with

$$R_0 = \rho_0 \, \text{tr}(\boldsymbol{L}^g) \,, \tag{38}$$

which allows us to explicitly calculate changes in mass in terms of the growth tensor $\boldsymbol{F}^g$. This approach is relatively common to characterize the mass increase in growing soft tissues such as arteries (Himpel et al., 2005) or skin (Buganza Tepole et al., 2011). Hard tissues, however, are typically characterized through an energy-driven evolution of the mass density, and the mass source R_0 is specified in terms of the referential mass density ρ_0 and the free energy ψ,

$$R_0 = k_\rho \left[\left[\frac{\rho_0}{\rho_0^*} \right]^{-m} \psi_0 - \psi_0^* \right] . \tag{39}$$

Herein, ρ_0^* and ψ_0^* denote the reference value of the density and of the free energy, m is an additional parameter to ensure algorithmic stability, and k_ρ has the unit of time divided by length squared to govern the speed of the adaption process, see Harrigan and Hamilton (1992) and Waffenschmidt and Menzel (2012) of this special issue. Typical examples of this type of density growth have been used extensively in the literature to characterize density profiles in the proxima femur (Kuhl et al., 2003; Kuhl and Steinmann, 2003c; Wolff, 1870), see Fig. 4. Additional applications include density profiles in the humerus of high performance athletes (Taylor et al., 2009), and density profiles in the proxima tibia in the context of osteoarthritis (Pang et al., 2012; Waffenschmidt et al., submitted for publication; Wolff, 1870), see Fig. 5.

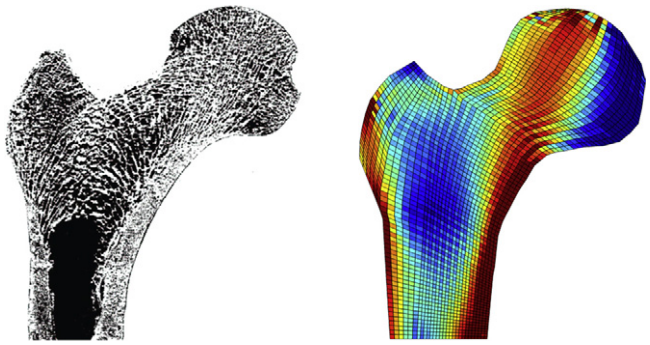

Fig. 4. Density growth of the proximal femur for an energy-driven mass source, $\dot{\rho}_0 = R_0$ with $R_0 = k_\rho[[\rho_0/\rho_0^*]^{-m}\psi_0 - \psi_0^*]$, according to Eqs. (17) and (39). Photograph of a thin section, left, demonstrates microstructural arrangement of trabeculae in the femur head aligned with the axis of maximum principal stress (Wolff, 1870). Computational simulation of density growth, right, predicts higher bone densities in regions of large mechanical stress and lower bone densities in unloaded regions (Kuhl et al., 2003; Kuhl and Steinmann, 2003c).

5.2. Mass flux

We can essentially distinguish two types of mass flux in open system thermodynamics; a gradient-based flow of matter which is typically associated with volume growth, and a surface-based flow of matter which is typically associated with surface growth. Gradient-based formulations are motivated in analogy to Fick's law of diffusion, or Fourier's law of heat conduction,

$$\boldsymbol{R} = \boldsymbol{D} \cdot \nabla_{\boldsymbol{X}} \rho_0 \quad \text{with} \quad \boldsymbol{D}(\boldsymbol{F}, \boldsymbol{F}^g, \boldsymbol{A}, \rho_0, \theta) \tag{40}$$

such that the symmetric conductivity tensor $\boldsymbol{D}$ maps the gradient of the referential mass density $\nabla_{\boldsymbol{X}} \rho_0$ onto the mass flux $\boldsymbol{R}$ (Kuhl et al., 2003). A typical example might be cell migration towards low density regions, e.g., in wound healing, with the goal to equilibrate density concentrations (Kuhl and Steinmann, 2004). Surface-based formulations can be motivated by the creation of new material at growing surfaces, which we have introduced as Γ in Section 2.3. If we denote their unit normal vector by $\boldsymbol{n}^\Gamma$, we can interpret surface growth as a flux of matter away from the surface Γ,

$$\boldsymbol{R} = \boldsymbol{D} \cdot \boldsymbol{n}^\Gamma \quad \text{with} \quad \boldsymbol{D}(\boldsymbol{F}, \boldsymbol{F}^g, \boldsymbol{A}, \rho_0, \theta) \tag{41}$$

such that the symmetric conductivity tensor $\boldsymbol{D}$ maps the normal $\boldsymbol{n}^\Gamma$ onto the mass flux $\boldsymbol{R}$ (Skalar et al., 1997). Typical examples

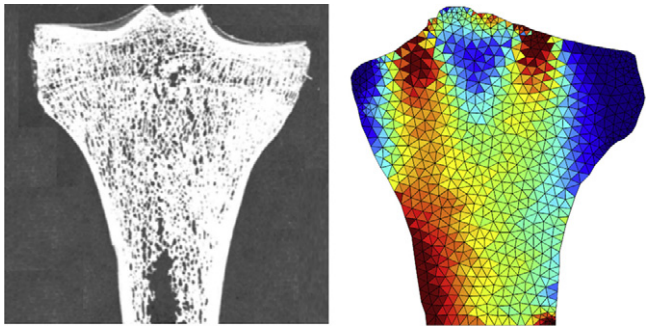

Fig. 5. Density growth of the proximal tibia for an energy-driven mass source, $\dot{\rho}_0 = R_0$ with $R_0 = k_\rho[[\rho_0/\rho_0^*]^{-m}\psi_0 - \psi_0^*]$, according to Eqs. (17) and (39). Photograph of a thin section, left, displays microstructural arrangement of trabeculae in the tibia head aligned with the axis of maximum principal stress (Wolff, 1870). Computational simulation of density growth, right, predicts a higher bone density in regions of large mechanical stress and lower bone density in unloaded regions (Pang et al., 2012; Waffenschmidt et al., submitted for publication).

of surfaces from which mass grows are nail beds, roots of hairs, or growth plates of long bones. In both cases, for the special case of transverse isotropy, the conductivity tensor takes the following explicit representation,

$$\boldsymbol{D} = \delta^{\text{iso}}\,\boldsymbol{I} + [\delta^{\text{ani}} - 1]\,\boldsymbol{n}\otimes\boldsymbol{n} \quad \text{with} \quad \boldsymbol{n} = \boldsymbol{a}/\|\boldsymbol{a}\|\,, \tag{42}$$

with the isotropic and anisotropic mass conduction coefficients δ^{iso} and δ^{ani}.

5.3. Momentum flux

The momentum flux is specified by a hyper-elastic form so that the Piola stresses are obtained from the derivative of the free energy function with respect to the deformation gradient. We assume the free energy to be an isotropic function, invariant under superposed rigid body motions. This implies that

$$\psi(\boldsymbol{F}, \boldsymbol{F}^{\text{g}}, \boldsymbol{A}, \rho_0, \theta) = \widehat{\psi}(\boldsymbol{C}^{\text{e}}, \widehat{\boldsymbol{A}}, \rho_0, \theta)\,, \tag{43}$$

with $\boldsymbol{C}^{\text{e}} = \boldsymbol{F}^{\text{et}}\cdot\boldsymbol{F}^{\text{e}}$ and $\widehat{\boldsymbol{A}} = \boldsymbol{F}^{\text{g}}\cdot\boldsymbol{A}\cdot\boldsymbol{F}^{\text{gt}} = \widehat{\boldsymbol{a}}\otimes\widehat{\boldsymbol{a}}$, such that $\check{\psi} = \widehat{\psi}$ is restricted to be a function of an irreducible set of invariants. Here, $\widehat{\boldsymbol{A}}$ and $\widehat{\boldsymbol{a}}$ can be interpreted as the push forward of the structural tensor $\boldsymbol{A}$ and of the vector $\boldsymbol{a}$, characterizing the microstructural orientation in the incompatible growth configuration. A possible set of strain invariants is the following

$$\begin{aligned}
&I_i^{\text{Ce}} = \text{tr}\,([\boldsymbol{C}^{\text{e}}]^i) && \text{for} \quad i = 1,2,3\\
&I_4^{\text{Ce}} = \text{tr}\,(\boldsymbol{C}^{\text{e}}\cdot\widehat{\boldsymbol{A}}) && I_5^{\text{Ce}} = \text{tr}\,([\boldsymbol{C}^{\text{e}}]^2\cdot\widehat{\boldsymbol{A}})\\
&I_6^{\text{Ce}} = \text{tr}\,(\boldsymbol{C}^{\text{e}}\cdot[\widehat{\boldsymbol{A}}]^2) && I_7^{\text{Ce}} = \text{tr}\,([\boldsymbol{C}^{\text{e}}]^2\cdot[\widehat{\boldsymbol{A}}]^2)\\
&I_j^{\widehat{A}} = \text{tr}\,([\widehat{\boldsymbol{A}}]^j) && \text{for} \quad j = 1,2,3.
\end{aligned} \tag{44}$$

Alternatively, we can represent the identical set of irreducible invariants in terms of spatial or material arguments, see (Menzel and Steinmann, 2003a,b) for a detailed discussion. Based on these considerations together with Eq. (28), the representation of the Piola stresses results in

$$\boldsymbol{P} = \boldsymbol{P}^{\text{e}}\cdot\boldsymbol{F}^{\text{g}-\text{t}} \quad \text{with}$$
$$\boldsymbol{P}^{\text{e}} = 2\rho_0\boldsymbol{F}^{\text{e}}\cdot\sum_{k=1}^{7}\frac{\partial\check{\psi}(I_k^{\text{Ce}}, I_{1,2,3}^{\widehat{A}}, \rho_0, \theta)}{\partial I_k^{\text{Ce}}}\frac{\partial I_k^{\text{Ce}}}{\partial\boldsymbol{C}^{\text{e}}}. \tag{45}$$

5.3.1. Isotropic elasticity

For the special case of an isotropic elastic response, the free energy function can be reduced to the following functional format in terms of the first three isotropic invariants only

$$\check{\psi}(I_{1,2,3}^{\text{Ce}}, \rho_0, \theta)\,. \tag{46}$$

Since the choice of the elastic baseline characterization strongly depends on the particular type of tissue, we do not further specify the free energy function at this stage, but refer the reader to Ogden (1997) and Schröder and Neff (2010) for further background information on non-linear isotropic elasticity.

5.3.2. Transversely isotropic elasticity

For the special case of a transversely isotropic elastic response for which both the growth tensor and the structural tensor are constant in time, i.e., $\boldsymbol{F}^{\text{g}} = \boldsymbol{I}$ and $\widehat{\boldsymbol{A}} = \boldsymbol{A}$, the free energy function can be reduced to account for five invariants only

$$\check{\psi}(I_{1,\ldots,5}^{\text{Ce}}, \rho_0, \theta). \tag{47}$$

For the general case of a transversely isotropic elastic response, the free energy could account for all ten invariants

$$\check{\psi}(I_{1,\ldots,7}^{\text{Ce}}, I_{1,2,3}^{\widehat{A}}, \rho_0, \theta)\,. \tag{48}$$

A typical example for an anisotropy-related strain-type deformation measure is the difference $I_4^{\text{Ce}} - I_1^{\widehat{A}}$. This strain measure vanishes identically for $\boldsymbol{C}^{\text{e}} = \boldsymbol{I}$, whereas $I_4^{\text{Ce}} - I_1'$ with $I_1' = \text{const}$ does generally not vanish in case of evolving structural tensors. The reader is referred to Boehler (1987), Holzapfel and Ogden (2003), Humphrey (2002) and Schröder and Neff (2010) for different aspects on the constitutive modeling of finite deformation anisotropic elasticity and particular examples of transversely isotropic free energy functions.

5.4. Evolution of growth

Three conceptually different approaches have been suggested to constitutively characterize the evolution of growth according to Eq. (30) or (31): the general tensor function concept, the homeostatic equilibrium concept, and the microstructural concept. While the former two approaches can, in principle, define a simultaneous growth and reorientation of the microstructural directions, the third approach allows us to address growth and reorientation individually. Since we believe this is the most versatile way of characterizing growing tissues with a pre-defined microstructure, we will introduce the first two concepts briefly and address the third one in more detail. For all three cases, the growth tensor $\boldsymbol{F}^{\text{g}}$ is commonly assumed to be equal to the identity tensor initially, i.e. $\boldsymbol{F}^{\text{g}}|_{t=0} = \boldsymbol{I}$, such that $\boldsymbol{F}^{\text{e}}|_{t=0} = \boldsymbol{F}$.

General tensorial evolution of growth. The general tensor function concept has traditionally been advocated by the continuum physics community (Imatani and Maugin, 2002). Using the concept of representation theorems (Boehler, 1987), a generic tensorial evolution equation for the growth tensor $\boldsymbol{F}^{\text{g}}$ is introduced. In accordance with the discussion in Remark 2, the growth tensor is restricted to by symmetric, i.e., $\boldsymbol{F}^{\text{g}} = \boldsymbol{U}^{\text{g}}$, and, moreover, assume isotropic hyperelasticity so that $\boldsymbol{M}^{\text{e}} = \boldsymbol{M}^{\text{et}}$. Accordingly, the evolution of growth can formally be introduced either in a stress-based form,

$$[\boldsymbol{L}^{\text{g}}]^{\text{sym}} = \vartheta_I^{\text{iso}}\,\boldsymbol{I} + \vartheta_M^{\text{iso}}\,\boldsymbol{M}^{\text{e}} + \vartheta_A^{\text{ani}}\,\widehat{\boldsymbol{A}} + \vartheta_{MA}^{\text{ani}}[\boldsymbol{M}^{\text{e}}\cdot\widehat{\boldsymbol{A}}]^{\text{sym}}\,, \tag{49}$$

or in a strain-based form,

$$[\boldsymbol{L}^{\text{g}}]^{\text{sym}} = \vartheta_I^{\text{iso}}\,\boldsymbol{I} + \vartheta_C^{\text{iso}}\,\boldsymbol{C}^{\text{e}} + \vartheta_A^{\text{ani}}\,\widehat{\boldsymbol{A}} + \vartheta_{CA}^{\text{ani}}[\boldsymbol{C}^{\text{e}}\cdot\widehat{\boldsymbol{A}}]^{\text{sym}}\,. \tag{50}$$

Here, for example, we have selected the elastic Mandel stresses $\boldsymbol{M}^{\text{e}}$ and the elastic right Cauchy Green tensor $\boldsymbol{C}^{\text{e}}$ as representative stress and strain measures to drive the growth process. The material parameters ϑ_I^{iso} and ϑ_A^{ani} characterize load-independent growth for both the stress- and strain-based case. While ϑ_I^{iso}, ϑ_C^{iso}, and ϑ_M^{iso} characterize isotropic growth, ϑ_A^{ani}, $\vartheta_{MA}^{\text{ani}}$, $\vartheta_{CA}^{\text{ani}}$ characterize anisotropic growth as these parameters weight contributions including the structural tensor $\widehat{\boldsymbol{A}}$.

Homeostatic equilibrium evolution of growth. The homeostatic equilibrium concept is typically advocated by the biomechanics community, since concepts of homeostatic stresses or strains take an intuitive interpretation in biochemistry. A generic evolution law based on a homeostatic stress state could take the following format,

$$\boldsymbol{L}^{\text{g}} = \mathbf{M}^{\text{e}} : [\boldsymbol{M}^{\text{e}} - \boldsymbol{M}_*^{\text{e}}] \tag{51}$$

where $\mathbf{M}^{\text{e}}$ denotes a fourth-order mobility tensor and $\boldsymbol{M}_*^{\text{e}}$ is a tensorial so-called target stress. Alternatively, we could formulate the evolution law based on a homeostatic strain state,

$$\boldsymbol{L}^{\text{g}} = \mathbf{C}^{\text{e}} : [\boldsymbol{C}^{\text{e}} - \boldsymbol{C}_*^{\text{e}}] \tag{52}$$

where $\mathbf{C}^{\text{e}}$ denotes a fourth-order mobility tensor and $\boldsymbol{C}_*^{\text{e}}$ is a tensorial target deformation. For the special case of volumetric target states, we can choose scalar-valued quantities such as pressure or dilation as homeostatic target stress M_*^{e} or target strain C_*^{e}. If we assume an isotropic mobility, such that the mobility tensors

are proportional to the fourth-order identity tensor with proportionality factors M^{e} and C^{e}, Eqs. (51) and (52) are of purely volumetric nature, i.e., $\boldsymbol{L}^{\mathrm{g}} = \mathsf{M}^{\mathrm{e}}[\boldsymbol{M}^{\mathrm{e}} : \boldsymbol{I} - M^{\mathrm{e}}_{*}]\boldsymbol{I}$ or $\boldsymbol{L}^{\mathrm{g}} = \mathsf{C}^{\mathrm{e}}[\boldsymbol{C}^{\mathrm{e}} : \boldsymbol{I} - C^{\mathrm{e}}_{*}]\boldsymbol{I}$, see (Schmid et al., 2012) for details. For the example of tumor growth, a fully tensorial stress-driven format, $\boldsymbol{L}^{\mathrm{g}} = -[\boldsymbol{\Sigma}^{\mathrm{e}} - \boldsymbol{\Sigma}^{\mathrm{e}}_{*}]$, based on the elastic Eshelby tensor $\boldsymbol{\Sigma}^{\mathrm{e}} = \psi_0\, \boldsymbol{I} - \boldsymbol{M}^{\mathrm{e}}$ is discussed in Ambrosi et al. (2012) of this special issue. For the example of glaucoma, i.e., growth and remodeling in the eye, a scalar stretch-driven format of collagen fibril growth towards a homeostatic equilibrium state is illustrated in Grytz et al. (2012) of this special issue.

Microstructural evolution of growth. The microstructural concept, which we will follow here, has been advocated by the material science community and by the theoretical and computational mechanics community, since it closely follows concepts introduced for crystal plasticity (Boyce et al., 1989; Lee, 1969; Naghdi, 1990). As outlined in Remark 1, this concept motivates the definition of the growth tensor by microstructural considerations. In analogy to Eq. (42), we formally incorporate the underlying microstructure through the structural tensor $\boldsymbol{A} = \boldsymbol{a} \otimes \boldsymbol{a}$ in terms of the microstructural direction $\boldsymbol{a}$,

$$\boldsymbol{F}^{\mathrm{g}} = \vartheta^{\mathrm{iso}}\,\boldsymbol{I} + [\vartheta^{\mathrm{ani}} - 1]\,\boldsymbol{n} \otimes \boldsymbol{n} \quad \text{with} \quad \boldsymbol{n} = \boldsymbol{a}/\|\boldsymbol{a}\|, \tag{53}$$

where ϑ^{iso} and ϑ^{ani} characterize the amount of isotropic and anisotropic growth, such that $\vartheta^{\mathrm{iso}}|_{t=0} = 1$ and $\vartheta^{\mathrm{ani}}|_{t=0} = 1$ in the initial ungrown state. Accordingly, we have $J^{\mathrm{g}} = [\vartheta^{\mathrm{iso}}]^2[\vartheta^{\mathrm{iso}} + \vartheta^{\mathrm{ani}} - 1]$, and $\boldsymbol{F}^{\mathrm{g}}|_{\vartheta^{\mathrm{iso}}=1,\,\vartheta^{\mathrm{ani}}=1} = \boldsymbol{I}$. The definition (53) implies that the growth tensor is a priori symmetric, $\boldsymbol{F}^{\mathrm{g}} = \boldsymbol{U}^{\mathrm{g}}$. As the rotational part of $\boldsymbol{F}^{\mathrm{g}}$ is neglected, $\boldsymbol{F}^{\mathrm{g}}$ transforms the direction vector $\boldsymbol{a}$ co-linearly to itself and scales $\boldsymbol{a}$ with the total amount of growth in this direction,

$$\widehat{\boldsymbol{a}} = \boldsymbol{F}^{\mathrm{g}} \cdot \boldsymbol{a} = [\vartheta^{\mathrm{iso}} + \vartheta^{\mathrm{ani}} - 1]\,\boldsymbol{a}\,. \tag{54}$$

With $\boldsymbol{n}$ constant in time, the material time derivative of growth can be expressed as follows

$$\dot{\boldsymbol{F}}^{\mathrm{g}} = \dot{\vartheta}^{\mathrm{iso}}\,\boldsymbol{I} + \dot{\vartheta}^{\mathrm{ani}}\,\boldsymbol{n} \otimes \boldsymbol{n}\,. \tag{55}$$

Using the Sherman–Morrison–Woodbury formula, we obtain the following explicit representation of the inverse of the growth tensor,

$$\boldsymbol{F}^{\mathrm{g}-1} = \frac{1}{\vartheta^{\mathrm{iso}}}\,\boldsymbol{I} - \frac{\vartheta^{\mathrm{ani}} - 1}{\vartheta^{\mathrm{iso}}[\vartheta^{\mathrm{iso}} + \vartheta^{\mathrm{ani}} - 1]}\,\boldsymbol{n} \otimes \boldsymbol{n} \tag{56}$$

for $\vartheta^{\mathrm{iso}} \neq 0$ and $\vartheta^{\mathrm{iso}} + \vartheta^{\mathrm{ani}} \neq 1$. Accordingly, we can derive the following explicit formulation for the growth velocity tensor

$$\boldsymbol{L}^{\mathrm{g}} = \frac{\dot{\vartheta}^{\mathrm{iso}}}{\vartheta^{\mathrm{iso}}}\,\boldsymbol{I} - \frac{\dot{\vartheta}^{\mathrm{iso}}[\vartheta^{\mathrm{ani}} - 1] - \vartheta^{\mathrm{iso}}\,\dot{\vartheta}^{\mathrm{ani}}}{\vartheta^{\mathrm{iso}}\,[\vartheta^{\mathrm{iso}} + \vartheta^{\mathrm{ani}} - 1]}\,\boldsymbol{n} \otimes \boldsymbol{n}\,. \tag{57}$$

The explicit evaluation of the growth part of the dissipation inequality (29)

$$\boldsymbol{M}^{\mathrm{e}} : \boldsymbol{L}^{\mathrm{g}} = \dot{\vartheta}^{\mathrm{iso}} \left[\frac{1}{\vartheta^{\mathrm{iso}}}\,\bar{I}_1^{M^{\mathrm{e}}} - \frac{\vartheta^{\mathrm{ani}} - 1}{\vartheta^{\mathrm{iso}}[\vartheta^{\mathrm{iso}} + \vartheta^{\mathrm{ani}} - 1]}\,\bar{I}_4^{M^{\mathrm{e}}} \right] + \dot{\vartheta}^{\mathrm{ani}} \left[\frac{1}{\vartheta^{\mathrm{iso}} + \vartheta^{\mathrm{ani}} - 1}\,\bar{I}_4^{M^{\mathrm{e}}} \right] \tag{58}$$

suggests to introduce the first term in brackets as the driving force for isotropic growth, ϑ^{iso}, and the second term in brackets as the driving force for anisotropic growth, ϑ^{ani}. Here, in analogy with the definitions in Eq. (44), we have introduced the first and fourth invariants of the Mandel stress, $\bar{I}_1^{M^{\mathrm{e}}} = \mathrm{tr}(\boldsymbol{M}^{\mathrm{e}})$ and $\bar{I}_4^{M^{\mathrm{e}}} = \mathrm{tr}(\boldsymbol{M}^{\mathrm{e}} \cdot [\boldsymbol{n} \otimes \boldsymbol{n}])$, which take the interpretation of the pressure and fiber stress. We could adopt a conceptually similar format

$$\boldsymbol{C}^{\mathrm{e}} : \boldsymbol{L}^{\mathrm{g}} = \dot{\vartheta}^{\mathrm{iso}} \left[\frac{1}{\vartheta^{\mathrm{iso}}}\,\bar{I}_1^{C^{\mathrm{e}}} - \frac{\vartheta^{\mathrm{ani}} - 1}{\vartheta^{\mathrm{iso}}[\vartheta^{\mathrm{iso}} + \vartheta^{\mathrm{ani}} - 1]}\,\bar{I}_4^{C^{\mathrm{e}}} \right] + \dot{\vartheta}^{\mathrm{ani}} \left[\frac{1}{\vartheta^{\mathrm{iso}} + \vartheta^{\mathrm{ani}} - 1}\,\bar{I}_4^{C^{\mathrm{e}}} \right] \tag{59}$$

to motivate the evolution of the growth multipliers for the case of microstructurally motivated strain-driven growth. Again, in analogy with Eq. (44), we have introduced the first and fourth invariants of the elastic right Cauchy Green deformation tensor, $\bar{I}_1^{C^{\mathrm{e}}} = \mathrm{tr}(\boldsymbol{C}^{\mathrm{e}})$ and $\bar{I}_4^{C^{\mathrm{e}}} = \mathrm{tr}(\boldsymbol{C}^{\mathrm{e}} \cdot [\boldsymbol{n} \otimes \boldsymbol{n}])$, which are associated with the volume change and fiber stretch. In the context of a vanishing mass flux contribution according to Eq. (38), the mass source reduces to the following expression

$$R_0 = \rho_0 \frac{3\,\dot{\vartheta}^{\mathrm{iso}}\vartheta^{\mathrm{iso}} + 2\dot{\vartheta}^{\mathrm{iso}}[\vartheta^{\mathrm{ani}} - 1] + \vartheta^{\mathrm{iso}}\dot{\vartheta}^{\mathrm{ani}}}{\vartheta^{\mathrm{iso}}[\vartheta^{\mathrm{iso}} + \vartheta^{\mathrm{ani}} - 1]}. \tag{60}$$

We will now elaborate three special cases of this general formulation for volume growth: isotropic growth, area growth, and fiber growth. We will specify the underlying kinematics, discuss possible driving forces for growth, and illustrate specific types of tissue for which the individual formulations can be used.

5.4.1. Volume growth

For the special case of isotropic growth, we characterize the growing tissue through a single isotropic growth multiplier ϑ^{g}, while the amount of anisotropic growth vanishes identically,

$$\vartheta^{\mathrm{iso}} = \vartheta^{\mathrm{g}} \qquad \text{and} \qquad \vartheta^{\mathrm{ani}} = 1. \tag{61}$$

This implies that Eq. (53) reduces to the following format,

$$\boldsymbol{F}^{\mathrm{g}} = \vartheta^{\mathrm{g}}\,\boldsymbol{I} \tag{62}$$

so that $J^{\mathrm{g}} = [\vartheta^{\mathrm{g}}]^3$ and $\boldsymbol{F}^{\mathrm{g}}|_{\vartheta^{\mathrm{g}}=1} = \boldsymbol{I}$. Along with the following explicit expressions for the inverse growth tensor according to Eq. (56),

$$\boldsymbol{F}^{\mathrm{g}-1} = \frac{1}{\vartheta^{\mathrm{g}}}\,\boldsymbol{I} \tag{63}$$

the definition of the growth velocity tensor reduces to the following expression according to Eq. (15),

$$\boldsymbol{L}^{\mathrm{g}} = \frac{\dot{\vartheta}^{\mathrm{g}}}{\vartheta^{\mathrm{g}}}\,\boldsymbol{I}\,. \tag{64}$$

The term of the dissipation inequality according to equation (58), and its strain based counterpart (59),

$$\boldsymbol{M}^{\mathrm{e}} : \boldsymbol{L}^{\mathrm{g}} = \frac{\dot{\vartheta}^{\mathrm{g}}}{\vartheta^{\mathrm{g}}}\,\bar{I}_1^{M^{\mathrm{e}}} \quad \text{or} \quad \boldsymbol{C}^{\mathrm{e}} : \boldsymbol{L}^{\mathrm{g}} = \frac{\dot{\vartheta}^{\mathrm{g}}}{\vartheta^{\mathrm{g}}}\,\bar{I}_1^{C^{\mathrm{e}}} \tag{65}$$

motivates the following stress- and strain-based evolution equations for growth

$$\dot{\vartheta}^{\mathrm{g}} = \frac{k_\vartheta}{\vartheta^{\mathrm{g}}}\,\bar{I}_1^{M^{\mathrm{e}}} \qquad \text{or} \qquad \dot{\vartheta}^{\mathrm{g}} = \frac{k_\vartheta}{\vartheta^{\mathrm{g}}}\,\bar{I}_1^{C^{\mathrm{e}}}, \tag{66}$$

where k_ϑ denotes a saturation-type target stress or strain function. The mass source, in the context of a vanishing mass flux and $\rho^{\mathrm{g}} \doteq \mathrm{const}$ according to e quation (38), takes the following simplified representation

$$R_0 = 3\,\rho_0\,\frac{\dot{\vartheta}^{\mathrm{g}}}{\vartheta^{\mathrm{g}}}\,. \tag{67}$$

Isotropic growth models are typically used to characterize growing tissue on a phenomenological level (Himpel et al., 2005; Schmid et al., 2012), as also demonstrated in Bellomo et al. (2012) of this special issue. Some typical examples addressed in the literature include growth of tumors (Ambrosi and Mollica, 2002), growing arteries (Kuhl et al., 2007), see Fig. 6, growing hearts of athletes (Göktepe et al., 2010b), growing hearts in general (Kroon et al.,

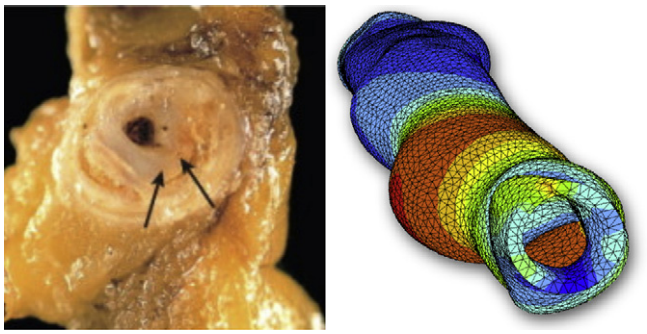

Fig. 6. Volume growth of an artery for stress-driven isotropic growth, $\boldsymbol{F}^{\mathrm{g}} = \vartheta^{\mathrm{g}}\,\boldsymbol{I}$ with $\dot{\vartheta}^{\mathrm{g}} = k_{\vartheta}\bar{I}_1^{M^{\mathrm{e}}}/\vartheta^{\mathrm{g}}$, according to Eqs. (62) and (66.1). Photograph of restenosis following balloon angioplasty, left, demonstrating residual atherosclerotic plaque and a new proliferative lesion caused by intimal thickening (Kumar et al., 2005). Computational simulation of isotropic volume growth, right, predicts wall thickening and re-narrowing of the lumen in response to stent-induced changes in the mechanical environment (Himpel et al., 2005; Kuhl et al., 2007).

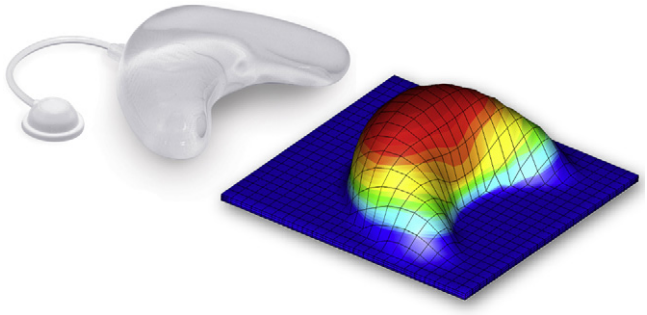

Fig. 7. Area growth of skin for stretch-driven transversely isotropic growth, $\boldsymbol{F}^{\mathrm{g}} = \sqrt{\vartheta^{\mathrm{g}}}\boldsymbol{I} + [1-\sqrt{\vartheta^{\mathrm{g}}}]\boldsymbol{n}\otimes\boldsymbol{n}$ with $\dot{\vartheta}^{\mathrm{g}} = k_{\vartheta}[\bar{I}_1^{C^{\mathrm{e}}} - \bar{I}_4^{C^{\mathrm{e}}}]/[2\,\vartheta^{\mathrm{g}}]$, according to Eqs. (69) and (73.2). Photograph of a tissue expander to induce controlled in situ skin growth for defect correction in reconstructive surgery, left, reprinted with permission, Mentor Worldwide LLC (Buganza Tepole et al., 2011). Computational simulation of transversely isotropic area growth, right, predicts area growth in response to controlled mechanical overstretch during tissue expansion (Buganza Tepole et al., in press).

2009), or the specific analysis of surface wrinkling in skin, as discussed in Ciarletta and BenAmar (2012) of this special issue.

5.4.2. Area growth

For the special case of transversely isotropic in-plane growth, for example present in growing biological membranes, the growth model becomes transversely isotropic. We can again characterize such growth phenomena through a single growth multiplier ϑ^{g}, which we can interpret as the in plane area growth, such that

$$\vartheta^{\mathrm{iso}} = \sqrt{\vartheta^{\mathrm{g}}} \quad \text{and} \quad \vartheta^{\mathrm{ani}} = 2 - \sqrt{\vartheta^{\mathrm{g}}}\,. \tag{68}$$

The generic growth tensor introduced in Eq. (53) then reduces to the following expression,

$$\boldsymbol{F}^{\mathrm{g}} = \sqrt{\vartheta^{\mathrm{g}}}\,\boldsymbol{I} + \left[1 - \sqrt{\vartheta^{\mathrm{g}}}\right]\ \boldsymbol{n}\otimes\boldsymbol{n} \tag{69}$$

so that $J^{\mathrm{g}} = \vartheta^{\mathrm{g}}$ and $\boldsymbol{F}^{\mathrm{g}}|_{\vartheta^{\mathrm{g}}=1} = \boldsymbol{I}$, which we can invert in closed form using Eq. (56)

$$\boldsymbol{F}^{\mathrm{g}-1} = \frac{1}{\sqrt{\vartheta^{\mathrm{g}}}}\,\boldsymbol{I} + \left[1 - \frac{1}{\sqrt{\vartheta^{\mathrm{g}}}}\right]\ \boldsymbol{n}\otimes\boldsymbol{n}\,. \tag{70}$$

This allows us to define the growth velocity tensor according to Eq. (15),

$$\boldsymbol{L}^{\mathrm{g}} = \frac{\dot{\sqrt{\vartheta}}^{\mathrm{g}}}{\sqrt{\vartheta}^{\mathrm{g}}}\,[\boldsymbol{I} - \boldsymbol{n}\otimes\boldsymbol{n}] = \frac{\dot{\vartheta}^{\mathrm{g}}}{2\,\vartheta^{\mathrm{g}}}\,[\boldsymbol{I} - \boldsymbol{n}\otimes\boldsymbol{n}]\,, \tag{71}$$

and to evaluate Eqs. (58) or (59)

$$\boldsymbol{M}^{\mathrm{e}} : \boldsymbol{L}^{\mathrm{g}} = \frac{\dot{\vartheta}^{\mathrm{g}}}{2\,\vartheta^{\mathrm{g}}}\,[\bar{I}_1^{M^{\mathrm{e}}} - \bar{I}_4^{M^{\mathrm{e}}}] \quad \text{or} \quad \boldsymbol{C}^{\mathrm{e}} : \boldsymbol{L}^{\mathrm{g}} = \frac{\dot{\vartheta}^{\mathrm{g}}}{2\,\vartheta^{\mathrm{g}}}\,[\bar{I}_1^{C^{\mathrm{e}}} - \bar{I}_4^{C^{\mathrm{e}}}] \tag{72}$$

to characterize possible stress- and strain-based evolution equations for growth

$$\dot{\vartheta}^{\mathrm{g}} = \frac{k_{\vartheta}}{2\,\vartheta^{\mathrm{g}}}\,[\bar{I}_1^{M^{\mathrm{e}}} - \bar{I}_4^{M^{\mathrm{e}}}] \quad \text{or} \quad \dot{\vartheta}^{\mathrm{g}} = \frac{k_{\vartheta}}{2\,\vartheta^{\mathrm{g}}}\,[\bar{I}_1^{C^{\mathrm{e}}} - \bar{I}_4^{C^{\mathrm{e}}}] \tag{73}$$

in terms of a saturation-type target stress or strain function k_{ϑ}. For the special case of a vanishing mass flux and $\rho^{\mathrm{g}} \doteq \text{const}$ according to Eq. (38), the mass source can be expressed as follows

$$R_0 = \rho_0\,\frac{\dot{\vartheta}^{\mathrm{g}}}{\vartheta^{\mathrm{g}}}\,. \tag{74}$$

Area growth of this form is characteristic for growing biological membranes. Issues of interest intensely discussed in the literature are instabilities in growing plates (Dervaux et al., 2009), membranes (Goriely and Tabor, 2003; McMahon et al., 2010), and shells (Goriely and BenAmar, 2005). Particular biomechanical applications include growing mucous membranes (Li et al., 2011) and growing skin (Buganza Tepole et al., 2011; Socci et al., 2007; Zöllner et al., 2012), see Figs. 7 and 8.

5.4.3. Fiber growth

For the special case of directional fiber growth, the growth model becomes transversely isotropic. We can again characterize growth in terms of a single growth multiplier ϑ^{g}, which we can interpret as the growth-induced fiber stretch,

$$\vartheta^{\mathrm{iso}} = 1 \quad \text{and} \quad \vartheta^{\mathrm{ani}} = \vartheta^{\mathrm{g}}\,. \tag{75}$$

Accordingly, the generic growth tensor of Eq. (53) reduces to the following expression

$$\boldsymbol{F}^{\mathrm{g}} = \boldsymbol{I} + [\vartheta^{\mathrm{g}} - 1]\boldsymbol{n}\otimes\boldsymbol{n}, \tag{76}$$

such that $J^{\mathrm{g}} = \vartheta^{\mathrm{g}}$ and $\boldsymbol{F}^{\mathrm{g}}|_{\vartheta^{\mathrm{g}}=1} = \boldsymbol{I}$. The explicit representation of its inverse according to Eq. (56) results in

$$\boldsymbol{F}^{\mathrm{g}-1} = \boldsymbol{I} - \frac{\vartheta^{\mathrm{g}} - 1}{\vartheta^{\mathrm{g}}}\,\boldsymbol{n}\otimes\boldsymbol{n} \tag{77}$$

and allows us to introduce the growth velocity tensor according to Eq. (15),

$$\boldsymbol{L}^{\mathrm{g}} = \frac{\dot{\vartheta}^{\mathrm{g}}}{\vartheta^{\mathrm{g}}}\,\boldsymbol{n}\otimes\boldsymbol{n}\,. \tag{78}$$

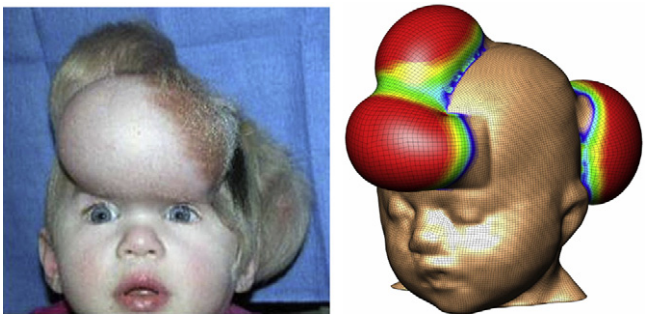

Fig. 8. Area growth of skin for stretch-driven transversely isotropic growth, $\boldsymbol{F}^{\mathrm{g}} = \sqrt{\vartheta^{\mathrm{g}}}\boldsymbol{I} + [1-\sqrt{\vartheta^{\mathrm{g}}}]\boldsymbol{n}\otimes\boldsymbol{n}$ with $\dot{\vartheta}^{\mathrm{g}} = k_{\vartheta}[\bar{I}_1^{C^{\mathrm{e}}} - \bar{I}_4^{C^{\mathrm{e}}}]/[2\vartheta^{\mathrm{g}}]$, according to Eqs. (69) and (73.2). Photograph of tissue expansion in pediatric forehead reconstruction, left, shows forehead, anterior and posterior scalp expansion to trigger skin growth in situ (Buganza Tepole et al., 2011; Gosain and Cortes, 2007). Computational simulation of transversely isotropic area growth, right, predicts area growth in response to controlled mechanical overstretch during tissue expansion (Zöllner et al., in press; Zöllner et al., 2012).

The driving force for growth according to Eq. (58) or (59),

$$\boldsymbol{M}^{\mathrm{e}} : \boldsymbol{L}^{\mathrm{g}} = \frac{\dot{\vartheta}^{\mathrm{g}}}{\vartheta^{\mathrm{g}}}\, \bar{I}_4^{M^{\mathrm{e}}} \quad \text{or} \quad \boldsymbol{C}^{\mathrm{e}} : \boldsymbol{L}^{\mathrm{g}} = \frac{\dot{\vartheta}^{\mathrm{g}}}{\vartheta^{\mathrm{g}}}\, \bar{I}_4^{C^{\mathrm{e}}} \tag{79}$$

may be combined with a saturation-type target stress or strain function k_ϑ, which motivates the following stress- and strain-based evolution equations for growth,

$$\dot{\vartheta}^{\mathrm{g}} = \frac{k_\vartheta}{\vartheta^{\mathrm{g}}}\, \bar{I}_4^{M^{\mathrm{e}}} \quad \text{or} \quad \dot{\vartheta}^{\mathrm{g}} = \frac{k_\vartheta}{\vartheta^{\mathrm{g}}}\, \bar{I}_4^{C^{\mathrm{e}}} \,. \tag{80}$$

In the context of a vanishing mass flux and $\rho^{\mathrm{g}} \doteq \text{const}$ according to Eq. (38), the mass source takes the representation

$$R_0 = \rho_0\, \frac{\dot{\vartheta}^{\mathrm{g}}}{\vartheta^{\mathrm{g}}} \,. \tag{81}$$

Fiber growth is characteristic for biological tissues, which grow along specific microstructural directions, as illustrated for one (Rodriguez et al., 1994) and three (Vandiver and Goriely, 2009) specific directions of anisotropy. Some typical examples include growing skeletal and cardiac muscle (Göktepe et al., 2010a; Rausch et al., 2011), as discussed in Kerckhoffs et al. (2012) and Klepach et al. (2012) of this special issue. Figs. 9 and 10 illustrate the associated cases of strain-driven cardiac dilation and stress-driven cardiac wall thickening (Göktepe et al., 2010a,b).

5.5. Evolution of structural tensor

While we have previously placed emphasis on the evolution of the growth tensor $\boldsymbol{F}^{\mathrm{g}}$ in the form of Eq. (53) with $\boldsymbol{n}$ remaining constant in time, we now address the evolution of the anisotropy direction itself. This reorientation model can easily be combined with the evolution of ϑ^{ani}. To specify the evolution of $\boldsymbol{n}$ in time, let us denote its initial orientation by $\boldsymbol{n}_0 = \boldsymbol{n}|_{t=0}$ and define its current orientation in terms of an orthogonal tensor $\boldsymbol{R}^n$,

$$\boldsymbol{n} = \boldsymbol{R}^n \cdot \boldsymbol{n}_0 \,. \tag{82}$$

This allows us to express the rate of $\boldsymbol{n}$ as

$$\dot{\boldsymbol{n}} = \dot{\boldsymbol{R}}^n \cdot \boldsymbol{n}_0 = \dot{\boldsymbol{R}}^n \cdot \boldsymbol{R}^{n\,\mathrm{t}} \cdot \boldsymbol{n} = \boldsymbol{\Omega}^n \cdot \boldsymbol{n} = \boldsymbol{\omega}^n \times \boldsymbol{n} \,, \tag{83}$$

where $\boldsymbol{\Omega}^n$ is the related spin tensor and $\boldsymbol{\omega}^n$ is its axial vector. By further specifying the axial vector $\boldsymbol{\omega}^n$, we can introduce an evolution equation for the microstructural orientation $\boldsymbol{n}$. We may, for instance, construct $\boldsymbol{\omega}^n$ in terms of a vector product, so that $\boldsymbol{n}$ aligns with a specific direction. Typical examples are either principal stress or principal strain directions. With the spectral decompositions

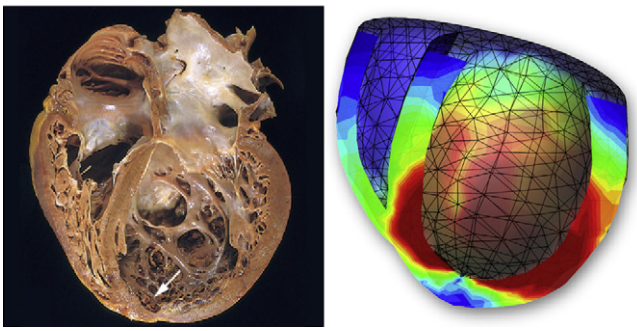

Fig. 9. Fiber growth of the heart for strain-driven transversely isotropic growth, $\boldsymbol{F}^{\mathrm{g}} = \boldsymbol{I} + [\vartheta^{\mathrm{g}} - 1]\, \boldsymbol{n} \otimes \boldsymbol{n}$ with $\dot{\vartheta}^{\mathrm{g}} = k_\vartheta \bar{I}_4^{C^{\mathrm{e}}} / \vartheta^{\mathrm{g}}$, according to Eqs. (76) and (80.2). Photograph of a heart in dilated cardiomyopathy, left, illustrates an increase in cavity size at a constant wall thickness, typically associated with volume-overload induced eccentric growth (Kumar et al., 2005). Computational simulation of transversely isotropic fiber growth, right, predicts an enlargement of the left ventricular cavity in response to mechanical overstretch (Göktepe et al., 2010a,b).

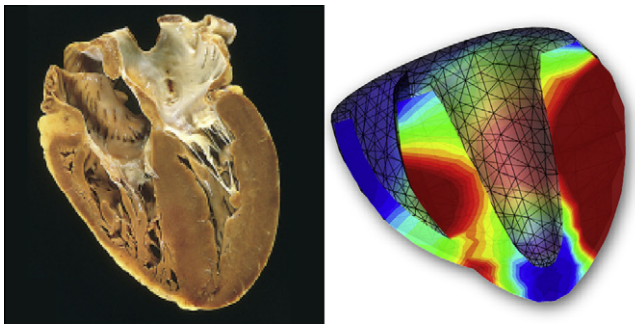

Fig. 10. Cross-fiber growth of the heart for stress-driven wall thickening, $\boldsymbol{F}^{\mathrm{g}} = \boldsymbol{I} + [\vartheta^{\mathrm{g}} - 1]\, \boldsymbol{n} \otimes \boldsymbol{n}$ with $\dot{\vartheta}^{\mathrm{g}} = k_\vartheta \bar{I}_1^{M^{\mathrm{e}}} / \vartheta^{\mathrm{g}}$, according to Eqs. (76) and (66.1). Photograph of a heart in hypertrophic cardiomyopathy, left, illustrates an increase in wall thickness at a constant cardiac size, typically associated with pressure-overload induced concentric growth (Kumar et al., 2005). Computational simulation of transversely isotropic cross-fiber growth, right, predicts a significant wall thickening of the left ventricular wall in response to hypertension (Göktepe et al., 2010a; Rausch et al., 2011).

$$\boldsymbol{M}^{\mathrm{e}} = M_i^{\mathrm{e}}\, \boldsymbol{m}_i^l \otimes \boldsymbol{m}_i^r \quad \text{or} \quad \boldsymbol{C}^{\mathrm{e}} = C_i^{\mathrm{e}}\, \boldsymbol{c}_i \otimes \boldsymbol{c}_i \tag{84}$$

we can express the reorientation of $\boldsymbol{n}$ either in a stress- or strain-driven form,

$$\boldsymbol{\omega}^n = \frac{1}{t_*}\, \boldsymbol{n} \times \boldsymbol{m} \quad \text{or} \quad \boldsymbol{\omega}^n = \frac{1}{t_*}\, \boldsymbol{n} \times \boldsymbol{c}, \tag{85}$$

where t_* represents a scaling parameter similar to the relaxation time in models for viscous bahavior. The vectors $\boldsymbol{m}$ and $\boldsymbol{c}$ represent particular directions associated with either $\boldsymbol{M}^{\mathrm{e}}$ or $\boldsymbol{C}^{\mathrm{e}}$, e.g., a direction associated with the maximum principal value $\max\{M_i^{\mathrm{e}}\}$ or $\max\{C_i^{\mathrm{e}}\}$. Since the form of reorientation model in Eq. (85) defines $\boldsymbol{\omega}^n$ perpendicular to the anisotropy direction $\boldsymbol{n}$ itself, so-called drilling rotations are a priori excluded (Betsch et al., 1998). By combining Eqs. (83) and (85) and using the $\varepsilon\,\delta$-rule we obtain the following representations of the evolution equations for the microstructural direction,

$$\dot{\boldsymbol{n}} = \frac{1}{t_*}[\boldsymbol{I} - \boldsymbol{n} \otimes \boldsymbol{n}] \cdot \boldsymbol{m} \quad \text{or} \quad \dot{\boldsymbol{n}} = \frac{1}{t_*}[\boldsymbol{I} - \boldsymbol{n} \otimes \boldsymbol{n}] \cdot \boldsymbol{c} \,. \tag{86}$$

From Eq. (86), we conclude that the constraint $\dot{\boldsymbol{n}} \cdot \boldsymbol{n} = 0$ is satisfied so that $\boldsymbol{n}$ remains a unit vector. Alternatively, we may also replace $\boldsymbol{m}$ or $\boldsymbol{c}$ in Eq. (86) with a stress- or strain-based mapping of the preferred direction $\boldsymbol{n}$ itself, which results in

$$\dot{\boldsymbol{n}} = \frac{1}{t_*}[\boldsymbol{I} - \boldsymbol{n} \otimes \boldsymbol{n}] \cdot \boldsymbol{M}^{\mathrm{e}} \cdot \boldsymbol{n} \quad \text{or} \quad \dot{\boldsymbol{n}} = \frac{1}{t_*}[\boldsymbol{I} - \boldsymbol{n} \otimes \boldsymbol{n}] \cdot \boldsymbol{C}^{\mathrm{e}} \cdot \boldsymbol{n}. \tag{87}$$

It is interesting to note that saturation-type evolution of the reorientation of $\boldsymbol{n}$ is directly implied in Eqs. (86) and (87): the rate of $\boldsymbol{n}$ goes to zero for $\boldsymbol{n}$ aligning with $\boldsymbol{m}$ or $\boldsymbol{c}$, or, respectively with $\boldsymbol{M}^{\mathrm{e}} \cdot \boldsymbol{n}$ or $\boldsymbol{C}^{\mathrm{e}} \cdot \boldsymbol{n}$. This indicates that both types of evolution equations, either (86) or (87), may result in one and the same stress- or strain-based reorientation direction as an alignment of $\boldsymbol{n}$ with $\boldsymbol{M}^{\mathrm{e}} \cdot \boldsymbol{n}$ or $\boldsymbol{C}^{\mathrm{e}} \cdot \boldsymbol{n}$ implies that $\boldsymbol{n}$ evolves towards a principal stress or strain direction. The evolution of the direction vector $\boldsymbol{n}$ also contributes to the dissipation inequality. For conceptual simplicity, consider the case where ϑ^{iso} and ϑ^{ani} do not evolve in time. The rate of the growth tensor then reduces to

$$\dot{\boldsymbol{F}}^{\mathrm{g}} = [\vartheta^{\mathrm{ani}} - 1]\, [\dot{\boldsymbol{n}} \otimes \boldsymbol{n} + \boldsymbol{n} \otimes \dot{\boldsymbol{n}}] \tag{88}$$

so that the growth velocity tensor takes the representation,

$$\boldsymbol{L}^{\mathrm{g}} = \frac{\vartheta^{\mathrm{ani}} - 1}{\vartheta^{\mathrm{iso}}}\, [\dot{\boldsymbol{n}} \otimes \boldsymbol{n} + \boldsymbol{n} \otimes \dot{\boldsymbol{n}}] - \frac{[\vartheta^{\mathrm{ani}} - 1]^2}{\vartheta^{\mathrm{iso}}[\vartheta^{\mathrm{iso}} + \vartheta^{\mathrm{ani}} - 1]}\, \dot{\boldsymbol{n}} \otimes \boldsymbol{n}. \tag{89}$$

Note that $\boldsymbol{L}^{\mathrm{g}}$ becomes unsymmetric due to the reorientation of $\boldsymbol{n}$ even though $\boldsymbol{F}^{\mathrm{g}}$ remains symmetric and the rotational part of

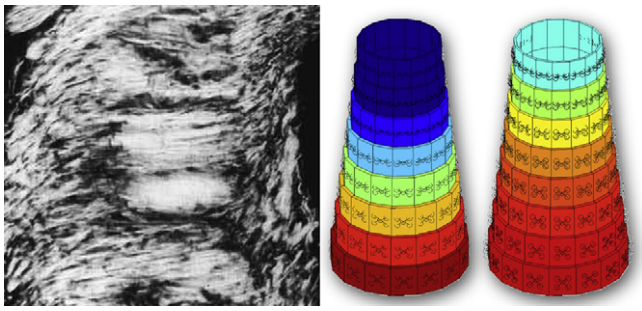

Fig. 11. Evolution of structural tensor in layered artery for stress- and strain-driven evolution of microstructural direction, $\dot{\boldsymbol{n}} = [\boldsymbol{I} - \boldsymbol{n} \otimes \boldsymbol{n}] \cdot \boldsymbol{M}^{\mathrm{e}} \cdot \boldsymbol{n}/t_*$ and $\dot{\boldsymbol{n}} = [\boldsymbol{I} - \boldsymbol{n} \otimes \boldsymbol{n}] \cdot \boldsymbol{C}^{\mathrm{e}} \cdot \boldsymbol{n}/t_*$ according to Eqs. (87.1) and (87.2). Polarized light micrograph of tangentially sectioned brain artery, left, showing variation of collagen fiber orientation from circumferential inner to helical outer layer (Finlay et al., 1995). Computational simulation of stress- and strain-driven fiber distribution, left and right, predicts a smooth variation of collagen fiber orientation from circumferential inner to helical outer layer (Kuhl et al., 2007).

$\boldsymbol{F}^{\mathrm{g}}$ is not activated, i.e., $\boldsymbol{R}^{\mathrm{g}} = \boldsymbol{I}$, see Remark 1. Accordingly, the unsymmetric part of $\boldsymbol{M}^{\mathrm{e}}$, as generally present in case of anisotropic elasticity, contributes to the growth-related dissipation part $\boldsymbol{M}^{\mathrm{e}} : \boldsymbol{L}^{\mathrm{g}}$. Evolving structural tensors have been applied successfully to explain characteristic tissue microstructures, for example in native arteries (Kuhl et al., 2007), see Fig. 11, and in the healthy heart, as discussed in Pluijmert et al. (2012) of this special issue. A reorientation of these native microstructures can be a severe problem in specific forms of disease, as illustrated for the case of glaucoma in the excellent overview (Grytz et al., 2012) of this special issue. Reproducing the correct native microstructural orientation is one of the biggest challenges in tissue engineering. Artificial tissue constructs grown in a dish are typically pre-conditioned to align their microstructural directions with either stress or strain to reproduce the native microstructure. Typical examples are tissue engineering of functional vascular grafts (Abilez et al., 2006), tendons or ligaments (Garikipati et al., 2004), with the particular example of a strain-driven reorientation along the maximum principal direction $\boldsymbol{c}$ according to equation (86.2) illustrated in Kuhl et al. (2005). For the algorithmic treatment of fiber reorientation the interested reader is referred to Himpel et al. (2008) and Menzel (2007).

Remark 4 *((Thermodynamically conjugate pairs)).* Here, we have evaluated the dissipation inequality (29) in terms of the elastic Mandel stress $\boldsymbol{M}^{\mathrm{e}}$ and the growth velocity tensor $\boldsymbol{L}^{\mathrm{g}}$ as thermodynamically conjugate pairs, introducing Eq. (58). Alternatively, we could introduce the Piola stress $\boldsymbol{P}^{\mathrm{g}} = -\rho_0 \partial_{\boldsymbol{F}^{\mathrm{g}}} \psi$ and the rate of the growth tensor $\dot{\boldsymbol{F}}^{\mathrm{g}}$ as thermodynamically conjugate pairs as introduced in Eq. (29), see also Remark 3. In view of the specific form of $\boldsymbol{F}^{\mathrm{g}}$ introduced in Eq. (53) and by assuming $\boldsymbol{n}$ to remain constant in time, we obtain

$$\boldsymbol{P}^{\mathrm{g}} : \dot{\boldsymbol{F}}^{\mathrm{g}} = \dot{\vartheta}^{\mathrm{iso}} \bar{I}_1^{\mathrm{pg}} + \dot{\vartheta}^{\mathrm{ani}} \bar{I}_4^{\mathrm{pg}} ,$$

where we have introduced the first and fourth invariant of the Piola stress, $\bar{I}_1^{\mathrm{pg}} = \mathrm{tr}(\boldsymbol{P}^{\mathrm{g}})$ and $\bar{I}_4^{\mathrm{pg}} = \mathrm{tr}(\boldsymbol{P}^{\mathrm{g}} \cdot [\boldsymbol{n} \otimes \boldsymbol{n}])$. In contrast to Eq. (58), the above equation clearly reflects the isotropic–anisotropic decoupling, with $\bar{I}_1^{\mathrm{pg}}$ acting as driving force for isotropic growth ϑ^{iso} and $\bar{I}_4^{\mathrm{pg}}$ acting as driving force for anisotropic growth ϑ^{ani}. This is not the case for the evaluation in terms of $\boldsymbol{M}^{\mathrm{e}}$ and $\boldsymbol{L}^{\mathrm{g}}$, see Eq. (58), where the driving forces for ϑ^{iso} depends on ϑ^{iso}, ϑ^{ani}, $\bar{I}_1^{M^{\mathrm{e}}}$, $\bar{I}_4^{M^{\mathrm{e}}}$ and the force driving ϑ^{ani} is a function of ϑ^{iso}, ϑ^{ani}, $\bar{I}_4^{M^{\mathrm{e}}}$.

Remark 5 *((Incompressibility and growth)).* Although it may appear rather trivial, there is a controversy of growth in combination with incompressibility (Schmid et al., 2012). The first possibility is to first perform the volumetric-isochoric decomposition of the total deformation gradient, $\boldsymbol{F} = J^{1/3} \overline{\boldsymbol{F}}$, where $\overline{\boldsymbol{F}} = j^{1/3} \boldsymbol{F}$, and then perform the multiplicative decomposition of the purely isochoric part, $\overline{\boldsymbol{F}} = \overline{\boldsymbol{F}}^{\mathrm{e}} \cdot \overline{\boldsymbol{F}}^{\mathrm{g}}$, i.e.,

$$\boldsymbol{F} = J^{1/3} \overline{\boldsymbol{F}}^{\mathrm{e}} \cdot \overline{\boldsymbol{F}}^{\mathrm{g}} .$$

Although computationally attractive, this approach is limited to the special case where growth remains purely isochoric, i.e., $J^{\mathrm{g}} = 1$, a case we have not discussed in the examples of this section. The second possibility is to first perform the multiplicative decomposition of the total deformation gradient, $\boldsymbol{F} = \boldsymbol{F}^{\mathrm{e}} \cdot \boldsymbol{F}^{\mathrm{g}}$, and then perform the volumetric-isochoric decomposition on the elastic part only, $\boldsymbol{F}^{\mathrm{e}} = J^{\mathrm{e}\,1/3} \overline{\boldsymbol{F}}^{\mathrm{e}}$, i.e.,

$$\boldsymbol{F} = J^{\mathrm{e}\,1/3} \overline{\boldsymbol{F}}^{\mathrm{e}} \cdot \boldsymbol{F}^{\mathrm{g}} .$$

Although most intuitive when growth is associated with volumetric changes, i.e., $J^{\mathrm{g}} \neq 1$, this approach may severely impact the algorithmic realization. It may require to reconsider existing computational algorithms, since elastic incompressibility can no longer be ensured on the element level by using existing element formulations that constrain the overall deformation to be incompressible, $J = 1$, or quasi-incompressible, $J \approx 1$.

6. Discussion

Research in the 1970s and 1980s, mainly lead by mechanical and bioengineering, has been driven by the quest for experimental evidence of growth and adaptation in hard tissues. Research in the 1990s, mainly lead by continuum mechanics and computational modeling, has allowed us to predict heterogeneous density profiles in agreement with these experimental findings. Research in the past decade has focused mainly on soft tissue growth. The community has grown exponentially from biologists, biophysicists, computer scientists, mathematicians, and engineers, to radiologists and clinicians in various disciplines. Right now, we are at the verge of appreciating that, in order to fully understand growth of biological tissues, we require a holistic and not just a reductionist view, we need mechanistic and not just phenomenological models, and we need to perform predictive and not just reproductive science.

Predictive modeling of biological growth is a challenging problem, but as mechanics community, we are optimally trained to face it: Modern continuum mechanics is multiscale, we are inherently passing information across the scales, most of our current models are not just phenomenological but microscopically motivated. Modern continuum mechanics is multifield, we are inherently passing information across the fields, most of our current field theories are based on coupled mechanical, thermal, electrical, and magnetic fields. The additional incorporation of biology and chemistry should, in principle, not introduce unresolvable difficulties. If we manage to understand mechanotransduction pathways in growth and remodeling, if we manage to integrate biomechanics and mechanobiology seamlessly into our models, and if we manage to manipulate these pathways systematically through a profound mechanistic understanding, our impact on life science and medicine could be tremendous. Continuum mechanics and computational mechanics have suffered from a severe identity crises within the past two decades. Growth and remodeling present an incredible opportunity to reposition our community at the forefront of science.

Acknowledgements

This work was supported by the National Science Foundation CAREER award CMMI-0952021 and by the National Institutes of Health Grant U54 GM072970.

References

Abilez, O., Benharash, P., Mehrotra, M., Miyamoto, E., Gale, A., Picquet, J., Xu, C., Zarins, C., 2006. A novel culture system shows that stem cells can be grown in 3D and under physiological pulsatile conditions for tissue engineering of vascular grafts. J. Surg. Res. 132, 170–178.

Alford, P.W., Taber, L.A., 2008. Computational study of growth and remodelling in the aortic arch. Comput. Methods Biomech. Biomed. Eng. 11, 525–538.

Alford, P.W., Humphrey, J.D., Taber, L.A., 2008. Growth and remodeling in a thick-walled artery model: effects of spatial variations in wall constituents. Biomech. Mod. Mechanobiol. 7, 245–262.

Alastrue, V., Martinez, M.A., Doblare, M., 2009a. Modelling adaptative volumetric finite growth in patient-specific residually stressed arteries. J. Biomech. 41, 1773–1781.

Alastrue, V., Martínez, M.A., Doblare, M., Menzel, A., 2009b. Anisotropic microsphere-based finite elasticity applied to blood vessel modelling. J. Mech. Phys. Solids 57, 178–203.

Ambrosi, D., Mollica, F., 2002. On the mechanics of a growing tumor. Int. J. Eng. Sci. 40, 1297–1316.

Ambrosi, D., Preziosi, L., Vitale, G., 2010. The insight of mixtures theory for growth and remodeling. ZAMP 61, 177–191.

Ambrosi, D., Ateshian, G.A., Arruda, E.M., Cowin, S.C., Dumais, J., Goriely, A., Holzapfel, G.A., Humphrey, J.D., Kemkemer, R., Kuhl, E., Olberding, J.E., Taber, L.A., Garikipati, K., 2011. Perspectives on biological growth and remodeling. J. Mech. Phys. Solids 59, 863–883.

Ambrosi, D., Preziosi, L., Vitale, G., 2012. The interplay between stress and growth in solid tumors. Mech. Res. Commun. 42, 87–91.

Arts, T., Reesink, K., Kroon, W., Delhaas, T., 2012. Simulation of adaptation of blood vessel geometry to flow and pressure: implications for arteriovenous impedance. Mech. Res. Commun. 42, 32–39.

Ateshian, G.A., Borrison, B., Holmes, J.W., Hung, C.T., 2012. Mechanics of cell growth. Mech. Res. Commun. 42, 118–125.

Bellomo, F.J., Armero, F., Nallim, L.G., Oller, S., 2012. A constitutive model for tissue adaptation: necrosis and stress driven growth. Mech. Res. Commun. 42, 51–59.

Ben Amar, M., Goriely, A., 2005. Growth and instability in elastic tissues. J. Mech. Phys. Solids 53, 2284–2319.

Betsch, P., Menzel, A., Stein, S., 1998. On the parameterization of finite rotations in computational mechanics. A classification of concepts with application to smooth shells. Comp. Methods Appl. Mech. Eng. 155, 273–305.

Boehler, J.P. (Ed.), 1987. Applications of Tensor Functions in Solid Mechanics. Number 292 in CISM Courses and Lectures. Springer.

Boyce, M.C., Weber, G.G., Parks, D.M., 1989. On the kinematics of finite strain plasticity. J. Mech. Phys. Solids 37, 647–665.

Buganza Tepole, A., Ploch, C.J., Wong, J., Gosain, A.K., Kuhl, E., 2011. Growin skin: a computational model for skin expansion in reconstructive surgery. J. Mech. Phys. Solids 59, 2177–2190.

Buganza, Tepole, A., Gosain, A.K., Kuhl, E. Stretching skin: the physiological limit and beyond. Int. J. Nonlin. Mech., doi:10.1016/j.ijnonlinmec.2011.07.006, in press.

Carter, D.R., Hayes, W.C., 1977. The behavior of bone as a twophase porous structure. J. Bone Joint Surg. 59, 7851/4794.

Chen, Y.C., Hoger, A., 2000. Constitutive functions of elastic materials in finite growth and deformation. J. Elast. 59, 175–193.

Ciarletta, P., BenAmar, M., 2012. Papillary networks in the dermalepidermal junction of skin: a biomechanical model. Mech. Res. Commun. 42, 68–76.

Ciarletta, P., Ambrosi, D., Maugin, G.A., 2012. Mass transport in morphogenetic processes: a second gradient theory for volumetric growth and material remodeling. J Mech. Phys. Solids 60, 525–537.

Cowin, S.C., Hegedus, D.H., 1977. Bone remodeling. 1. Theory of adaptive elasticity. J. Elast. 6, 313–326.

Cowin, S.C., 2004. Tissue growth and remodeling. Ann. Rev. Biomed. Eng. 6, 77–107.

Dassiso, G., Lindel, I.V., 2001. On the Helmholtz decomposition for polyadics. Quart. Appl. Math. 59, 787–796.

Dervaux, J., Ciarletta, P., Ben Amar, M., 2009. Morphogenesis of thin hyperelastic plates: a constitutive theory of biological growth in the Föppl-von Karman limit. J. Mech. Phys. Solids 57, 458–471.

Dumais, J., Shaw, S.L., Steele, C.R., Long, S.R., Ray, P.M., 2006. An anisotropic–viscoplastic model of plant cell morphogenesis by tip growth. Int. J. Dev. Biol. 50, 209–222.

Epstein, M., Maugin, G.A., 2000. Thermomechanics of volumetric growth in uniform bodies. Int. J. Plast. 16, 951–978.

Famaey, N., Vander Sloten, J., Kuhl, E. A three-constituent damage model for arterial clamping in computer-assisted surgery, Biomech. Mod. Mechanobio., doi:10.1007/s10237-012-0386-7, in press.

Finlay, H.M., McCullough, L., Canham, P.B., 1995. Three-dimensional collagen organization of human brain arteries at different transmural pressures. J. Vas. Res. 30, 1–312.

Garikipati, K., Arruda, E.M., Grosh, K., Narayanan, H., Calve, S., 2004. A continuum treatment of growth in biological tissue: the coupling of mass transport and mechanics. J. Mech. Phys. Solids 159, 5–1625.

Garikipati, K., 2009. The kinematics of biological growth. Appl. Mech. Rev. 62, 030801.1–030801.7.

Gibson, L.J., Ashby, M.F., 1997. The mechanics of three-dimensional cellular materials. Proc. R. Soc. London A 382, 43–59.

Göktepe, S., Abilez, O.J., Parker, K.K., Kuhl, E., 2010a. A multiscale model for eccentric and concentric cardiac growth through sarcomerogenesis. J. Theor. Biol. 265, 433–442.

Göktepe, S., Abilez, O.J., Kuhl, E., 2010b. A generic approach towards finite growth with examples of athlete's heart, cardiac dilation, and cardiac wall thickening. J. Mech. Phys. Solids 58, 1661–1680.

Goriely, A., Tabor, M., 2003. Biomechanical models of hyphal growth in actinomycetes. J. Theor. Biol. 222, 2111/4218.

Goriely, A., BenAmar, M., 2005. Differential growth and instability in elastic shells. Phys. Rev. Lett. 94, 198103.

Goriely, A., BenAmar, M., 2007. On the definition and modeling of incremental, cumulative, and continuous growth laws in morphoelasticity. Biomech. Mod. Mechanobiol. 6, 2891/4296.

Gosain, A.K., Cortes, W., 2007. Pediatric tissue expansion for forehead reconstruction: a 13-year review and an algorithm for its use. Am. Soc. Plast Surg. Baltimore, Abstract 13288.

Grytz, R., Girkin, C.A., Libertiaux, V., Downs, J.C., 2012. Perspectives on biomechanical growth and remodeling mechanisms in glaucoma. Mech. Res. Commun. 42, 92–106.

Harrigan, T.P., Hamilton, J.J., 1992. An analytical and numerical study of the stability of bone remodelling theories: dependence on microstructural stimulus. J. Biomech. 25, 477–488, Corrigendum, 1993;26:365–366.

Harrysson, M., Ristinmaa, M., Wallin, M., Menzel, A., 2010. Framework for deformation induced anisotropy in glassy polymers. Acta Mech. 211, 195–213.

Himpel, G., Kuhl, E., Menzel, A., Steinmann, P., 2005. Computational modeling of isotropic multiplicative growth. Comp. Mod. Eng. Sci. 8, 119–134.

Himpel, G., Menzel, A., Kuhl, E., Steinmann, P., 2008. Time-dependent fiber reorientation of transversely isotropic continua-finite element formulation and consistent linearization. Int. J. Num. Methods Eng. 73, 1413–1433.

Hoger, A., 1996. The elasticity tensor of a transversely isotropic hyperelastic material with residual stress. J. Elast. 42, 115–132.

Holzapfel, G.A., Ogden, R.W. (Eds.), 2003. Biomechanics of Soft Tissue in Cardiovascular Systems. Number 441 in CISM Courses and Lectures. Springer.

Hsu, H.F., 1968. The influence of mechanical loads on the form of a growing elastic body. J. Biomech. 1, 303–311.

Humphrey, J.D., 2001. Stress, strain, and mechanotransduction in cells. J. Biomech. Eng. 123, 638–641.

Humphrey, J.D., 2002. Cardiovascular Tissue Mechanics: Cells, Tissues, and Organs. Springer.

Humphrey, J.D., Rajagopal, K.R., 2002. A constrained mixture model for growth and remodeling of soft tissues. Math. Mod. Methods Appl. Sci. 12, 407–430.

Imatani, S., Maugin, G.A., 2002. A constitutive model for material growth and its application to three-dimensional finite element analysis. Mech. Res. Commun. 29, 477–483.

Isaksson, H., 2012. Recent advances in mechanobiological modeling of bone regeneration. Mech. Res. Commun. 42, 22–31.

Itoh, A., Krishnamurthy, G., Swanson, J., Ennis, D., Bothe, W., Kuhl, E., Karlsson, M., Davis, L., Miller, D.C., Ingels, N.B., 2009. Active stiffening of mitral valve leaflets in the beating heart. Am. J. Physiol. Heart Circ. Physiol. 296, 1766–1773.

Jaalouk, D.E., Lammerding, J., 2009. Mechanotransduction gone awry. Nat. Rev. Mol. Cell Biol. 10, 63–73.

Kerckhoffs, R., Omens, J., McCulloch, A.D., 2012. A single strain-based growth law predicts concentric and eccentric cardiac growth during pressure and volume overload. Mech. Res. Commun. 42, 40–50.

Klepach, D., Lee, L.C., Wenk, J.F., Ratcliffe, M.B., Zohdi, T.I., Navia, J.L., Kassab, G.S., Kuhl, E., Guccione, J.M., 2012. Growth and remodeling of the left ventricle: a case study of myocardial infarction and surgical ventricular restoration. Mech. Res. Commun. 42, 134–141.

Krishnamurthy, G., Ennis, D.B., Itoh, A., Bothe, W., Swanson-Birchill, J.C., Karlsson, M., Kuhl, E., Miller, D.C., Ingels, N.B., 2008. Material properties of the ovine mitral valve anterior leaflet in vivo from inverse finite element analysis. Am. J. Physiol. Heart Circ. Physiol. 295, H1141–H1149.

Kroeger, J., Daher, F.B., Grant, M., Geitmann, A., 2009. Microfilament orientation contrains vesicle flow and spatial distribution in growing pollen tubes. Biophys. J. 97, 1822–1831.

Kroeger, J., Geitmann, A., 2012. Pollen tube growth: getting a grip on cell biology through modeling. Mech. Res. Commun. 42, 32–39.

Kröner, E.,1981. Continuum theory of defects. In: Physics of Defects. North-Holland, pp. 215–315.

Kroon, W., Delhaas, T., Arts, T., Bovendeerd, P., 2009. Computational modeling of volumetric soft tissue growth: application to the cardiac left ventricle. Biomech. Mod. Mechanobiol. 8, 309–310.

Kuhl, E., Steinmann, P., 2003a. Mass- and volume specific views on thermodynamics for open systems. Proc. R. Soc. 459, 2547–2568.

Kuhl, E., Steinmann, P., 2003b. On spatial and material settings of thermohyperelastodynamics for open systems. Acta Mech. 160, 179–217.

Kuhl, E., Menzel, A., Steinmann, P., 2003. Computational modeling of growth—a critical review, a classification of concepts and two new consistent approaches. Comp. Mech. 32, 71–88.

Kuhl, E., Steinmann, P.P., 2003c. Theory and numerics of geometrically nonlinear open systems. Int. J. Num. Methods Eng. 58, 1593–1615.

Kuhl, E., Steinmann, P., 2004. Computational modeling of healing—an application of the material force method. Biomech. Mod. Mechanobiol. 2, 187–203.

Kuhl, E., Garikipati, K., Arruda, E.M., Grosh, K., 2005. Remodeling of biological tissue—mechanically induced reorientation of a transversely isotropic chain network. J. Mech. Phys. Solids 53, 1552–1573.

Kuhl, E., Maas, R., Himpel, G., Menzel, A., 2007. Computational modeling of arterial wall growth: attempts towards patient-specific simulations based on computer tomography. Biomech. Mod. Mechanobiol. 6, 321–331.

Kuhl, E., Holzapfel, G.A., 2007. A continuum model for remodeling in living structures. J. Mater. Sci. 42, 8811–8823.
Kumar, V., Abbas, A.K., Fausto, N., 2005. Robbins and Cotran Pathologic Basis of Disease. Elsevier Saunders.
Lee, E.H., 1969. Elastic-plastic deformation at finite strains. J. Appl. Mech. 36, 1–6.
Li, B., Cao, Y.P., Feng, X.Q., Gao, H., 2011. Surface wrinkling of mucosa induced by volumetric growth: theory, simulation and experiment. J. Mech. Phys. Solids 59, 758–774.
Lodge, A.S., 1974. Body Tensor Fields in Continuum Mechanics—With Application to Polymer Rheology. Academic Press.
Lubarda, A., Hoger, A., 2002. On the mechanics of solids with a growing mass. Int. J. Solids Struct. 39, 4627–4664.
Lubarda, V.A., 2004. Constitutive theories based on the multiplicative decomposition of deformation gradient: thermoelasticity, elastoplasticity and biomechanics. Appl. Mech. Rev. 57, 951/4108.
McMahon, J., Goriely, A., Tabor, M., 2010. Spontaneous cavitation in growing elastic membranes. Math. Mech. Solids 15, 57–77.
Menzel, A., 2005. Modelling of anisotropic growth in biological tissues—a new approach and computational aspects. Biomech. Mod. Mechanobiol. 3, 147–171.
Menzel, A., 2007. A fibre reorientation model for orthotropic multiplicative growth. Biomech. Mod. Mechanobiol. 6, 303–320.
Menzel, A., Harrysson, M., Ristinmaa, M., 2008. Towards an orientation-distribution-based multi-scale approach for remodelling biological tissues. Comput. Methods Biomech. Biomed. Eng. 11, 505–524.
Menzel, A., Steinmann, P., 2000. On the continuum formulation of higher gradient plasticity for single and polycrystals. J. Mech. Phys. Solids 48, 1777–1796, Erratum, 2001;49:1179–1180.
Menzel, A., Steinmann, P., 2003a. A view on anisotropic finite hyper-elasticity. Eur. J. Methods A/Solids 22, 71–87.
Menzel, A., Steinmann, P., 2003b. On the spatial formulation of anisotropic multiplicative elasto-plasticity. Comput. Methods Appl. Mech. Eng. 192, 3431–3470.
Menzel, A., Waffenschmidt, T., 2009. A micro-sphere-based remodelling formulation for anisotropic biological tissues. Philos. Trans. R. Soc. A 367, 3499–3523.
Moulton, D.E., Goriely, A., 2011. Circumferential buckling instability of a growing cylindrical tube. J. Mech. Phys. Solids 59, 525–537.
Mow, V.C., Holmes, M.H., Lai, W.M., 1984. Fluid transport and mechanical properties of articular cartilage—a review. J. Biomech. 17, 377–394.
Murtada, S.I., Kroon, M., Holzapfel, G.A., 2010. A calcium-driven mechanochemical model for prediction of force generation in smooth muscle. Biomech. Mod. Mechanobiol. 9, 7491/4762.
Naghdi, P., 1990. A critical review of the state of finite plasticity. J. Appl. Math. Phys. 41, 315–394.
Noll, W., 1967. Materially uniform simple bodies with inhomogeneities. Arch. Rational Mech. Anal. 27, 1–32, Errata. Noll W, Toupin RA, Wang CC. Arch Rational Mech. Anal. 1968;31:401.
Ogden, R.W., 1997. Non-Linear Elastic Deformations. Dover.
Olver, P.J., 1993. Application of Lie Groups to Differential Equations, volume 107 of Graduate Texts in Mathematics, 2nd edition. Springer.
Pang, H., Shiwalkar, A.P., Madormo, C.M., Taylor, R.E., Andriacchi, T.P., Kuhl, E., 2012. Computational modeling of bone density profiles in response to gait: A subject-specific approach. Biomech. Mod. Mechanobiol. 11, 379–390.
Pluijmert, M., Kroon, W., Delhaas, T., Bovendeerd, P., 2012. Adaptive reorientation of cardiac myofibers: the long-term effect on initial and boundary conditions. Mech. Res. Commun. 42, 60–67.
Preziosi, L., Tosin, A.R., 2009. Multiphase modelling of tumour growth and extracellular matrix interaction: mathematical tools and applications. J. Math. Biol. 58, 625–656.
Rausch, M.K., Dam, A., Göktepe, S., Abilez, O.J., Kuhl, E., 2011. Computational modeling of growth: systemic and pulmonary hypertension in the heart. Biomech. Mod. Mechanobiol. 10, 799–811.
Rodriguez, E.K., Hoger, A., McCulloch, A.D., 1994. Stress-dependent finite growth in soft elastic tissues. J. Biomech. 27, 455–467.
Schmid, H., Pauli, L., Paulus, A., Kuhl, E., Itskov, M., 2012. How to utilise the kinematic constraint of incompressibility for modelling adaptation of soft tissues. Comp. Methods Biomech. Biomed. Eng., doi:10.1080/10255842.2010.548325.
Schröder, J., Neff, P. (Eds.), 2010. Poly-, Quasi- and Rank-One Convexity in Applied Mechanics. Number 516 in CISM Courses and Lectures. Springer.
Šilhavý, M., 1997. The Mechanics and Thermomechanics of Continuous Media. Texts and Monographs in Physics. Springer.
Skalak, R., 1981. Growth as a finite displacement field. In: IUTAM Symposium on Finite Elasticity. Martinus Nijhoff, pp. 347–355.
Skalar, R., Farrow, D.A., Hoger, A., 1997. Kinematics of surface growth. J. Math. Biol. 35, 869–907.
Socci, L., Rennati, G., Gervaso, F., Vena, P., 2007. An axisymmetric computational model of skin expansion and growth. Biomech. Mod. Mechanobiol. 6, 177–188.
Taber, L.A., 1995. Biomechanics of growth, remodeling and morphogenesis. Appl. Mech. Rev. 48, 487–545.
Taber, L.A., Humphrey, J.D., 2001. Stress-modulated growth, residual stress, and vascular heterogeneity. J. Biomech. Eng. 123, 528–535.
Taylor, R.E., Zheng, C., Jackson, P.R., Doll, J.C., Chen, J.C., Holzbaur, K.R.S., Besier, T., Kuhl, E., 2009. The phenomenon of twisted growth: humeral torsion in dominant arms of high performance tennis players. Comp. Methods Biomech. Biomed. Eng. 12, 83–93.
Thompson, A.W., 1917. On Growth and Form. Cambridge University Press.
Tsamis, A., Cheng, A., Nguyen, T.C., Langer, F., Miller, D.C., Kuhl, E., 2012. Kinematics of cardiac growth–in vivo characterization of growth tensors and strains. J. Mech. Behav. Biomed. Mater. 8, 165–177.
Valentin, A., Holzapfel, G.A., 2012. Constrained mixture models as tools for testing competing hypotheses in arterial biomechanics: a survey. Mech. Res. Commun. 42, 126–133.
Vandiver, R., Goriely, A., 2009. Differential growth and residual stress in cylindrical elastic structures. Philos. Trans. R. Soc. A 367, 3607–3630.
Verdier, C., Etienne, J., Duperray, A., Preziosi, L., 2009. Review: rheological properties of biological materials. Comptes Rendus Phys. 10, 790–811.
Waffenschmidt, T., Menzel, A., Kuhl, E. Anisotropic density growth of bone. A computational micro-sphere approach. Submitted for publication.
Waffenschmidt, T., Menzel, A., 2012. Application of an anisotropic growth and remodeling formulation to computational topology optimization. Mech. Res. Commun. 42, 77–86.
Wolff, J., 1870. Über die innere Architectur der Knochen und ihre Bedeutung für die Frage vom Knochenwachstum. Virchows Archiv für Pathologische Anatomie und Physiologie und für Klinische Medizin 50, 389–453.
Wong, V.W., Akaishi, S., Longaker, M.T., Gurtner, G.C., 2011. Pushing back: wound mechanotransduction in repair and regeneration. J. Invest. Dermatol., doi:10.1038/jid.201.212.
Zeinali-Davarani, S., Baek, S., 2012. Medical image-based simulation of abdominal aortic aneurysm growth. Mech. Res. Commun. 42, 107–117.
Zöllner, A.M., Buganza, T.A., Gosain, A.K., Kuhl, E. Growing skin—tissue expansion in pediatric forehead reconstruction. Biomech. Mod. Mechanobiol., doi:10.1007/s10237-011-0357-4, in press.
Zöllner, A.M., Buganza Tepole, A., Kuhl, E., 2012. On the biomechanics and mechanobiology of growing skin. J. Theor. Biol. 297, 166–175.